Neurobiology of Disease 165 (2022) 105649

Contents lists available at ScienceDirect

Neurobiology of Disease

journal homepage: www.elsevier.com/locate/ynbdi

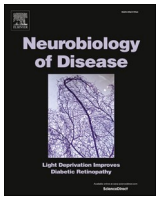

Vitamin E prevents lipid peroxidation and iron accumulation in *PLA2G6*-Associated Neurodegeneration

Irene Villalón-García [a], Mónica Álvarez-Córdoba [a], Suleva Povea-Cabello [a], Marta Talaverón-Rey [a], Marina Villanueva-Paz [a], Raquel Luzón-Hidalgo [a], Juan M. Suárez-Rivero [a], Alejandra Suárez-Carrillo [a], Manuel Munuera-Cabeza [a], Joaquín J. Salas [b], Rafael Falcón-Moya [c], Antonio Rodríguez-Moreno [c], José A. Armengol [d], José A. Sánchez-Alcázar [a,*]

[a] *Centro Andaluz de Biología del Desarrollo (CABD-CSIC-Universidad Pablo de Olavide de Sevilla), and Centro de Investigación Biomédica en Red: Enfermedades Raras, Instituto de Salud Carlos III, Spain*
[b] *Departamento de Bioquímica y Biología Molecular de Productos Vegetales, Instituto de la Grasa (CSIC), Sevilla, Spain*
[c] *Laboratorio de Neurociencia Celular y Plasticidad, Departamento de Fisiología, Anatomía y Biología Celular, Universidad Pablo de Olavide, Sevilla, Spain*
[d] *Departamento de Fisiología, Anatomía y Biología Celular, Universidad Pablo de Olavide, Sevilla, Spain*

ARTICLE INFO

Keywords:
PLA2G6-Associated Neurodegeneration
NBIA
Lipid peroxidation
Vitamin E
Iron accumulation
Mitochondria
Lipofuscin

ABSTRACT

Background: *PLA2G6*-Associated Neurodegeneration (PLAN) is a rare neurodegenerative disease with autosomal recessive inheritance, which belongs to the NBIA (Neurodegeneration with Brain Iron Accumulation) group. Although the pathogenesis of the disease remains largely unclear, lipid peroxidation seems to play a central role in the pathogenesis. Currently, there is no cure for the disease.

Objective: In this work, we examined the presence of lipid peroxidation, iron accumulation and mitochondrial dysfunction in two cellular models of PLAN, patients-derived fibroblasts and induced neurons, and assessed the effects of α-tocopherol (vitamin E) in correcting the pathophysiological alterations in PLAN cell cultures.

Methods: Pathophysiological alterations were examined in fibroblasts and induced neurons generated by direct reprograming. Iron and lipofuscin accumulation were assessed using light and electron microscopy, as well as biochemical analysis techniques. Reactive Oxygen species production, lipid peroxidation and mitochondrial dysfunction were measured using specific fluorescent probes analysed by fluorescence microscopy and flow cytometry.

Results: PLAN fibroblasts and induced neurons clearly showed increased lipid peroxidation, iron accumulation and altered mitochondrial membrane potential. All these pathological features were reverted with vitamin E treatment.

Conclusions: PLAN fibroblasts and induced neurons reproduce the main pathological alterations of the disease and provide useful tools for disease modelling. The main pathological alterations were corrected by Vitamin E supplementation in both models, suggesting that blocking lipid peroxidation progression is a critical therapeutic target.

Abbreviations: ΔΨm, mitochondrial membrane potential; ANAD, Atypical Neuroaxonal Dystrophy; (*S*)-BEL, S-Bromoenol Lactone; *BPAN*, Beta-Propeller Protein-Associated Neurodegeneration; CCCP, Carbonyl Cyanide Chlorophenylhydrazone; DMEM, Dulbecco's modified Eagle's medium; D-PUFAs, Deuterated Poly-unsaturated Fatty Acids; ICP-MS, inductively coupled plasma mass spectrometry; INAD, Infantile Neuroaxonal Dystrophy; iNs, Induced neurons; iPLA2β, calcium-independent Phospholipase A2 group VI; *NBIA*, Neurodegeneration with Brain Iron Accumulation; *PKAN*, *Pantothenate Kinase-associated Neurodegeneration*; *PLAN*, *PLA2G6-associated Neurodegeneration*; PPB, Perl's Prussian Blue; ROS, Reactive oxygen species; SBB, Sudan Black B.

* Corresponding author at: Centro Andaluz de Biología del Desarrollo (CABD), Consejo Superior de Investigaciones Científicas. Universidad Pablo de Olavide, Carretera de Utrera Km 1, Sevilla 41013, Spain.

E-mail addresses: jjsalas@ig.csic.es (J.J. Salas), rfalmoy@acu.upo.es (R. Falcón-Moya), arodmor@upo.es (A. Rodríguez-Moreno), jaarmbut@upo.es (J.A. Armengol), jasanalc@upo.es (J.A. Sánchez-Alcázar).

https://doi.org/10.1016/j.nbd.2022.105649
Received 14 November 2021; Received in revised form 11 January 2022; Accepted 31 January 2022
Available online 2 February 2022

1. Introduction

Neurodegeneration with Brain Iron Accumulation (NBIA) is a group of rare genetic diseases that cause progressive neurodegeneration. NBIA patients present radiological evidence of iron accumulation in certain brain areas (Gregory and Hayflick, 2013; Gregory and Hayflick, 2005). Currently, there are fifteen genes associated with NBIA disorders (Levi and Tiranti, 2019). The two more frequent NBIA subtypes are Pantothenate Kinase-associated Neurodegeneration (PKAN) and Beta-Propeller Protein-Associated Neurodegeneration (BPAN) (Gregory and Hayflick, 2013; Levi and Tiranti, 2019); while *PLA2G6*-Associated Neurodegeneration (PLAN) is the third more prevalent mutation of NBIA diseases (Gregory and Hayflick, 2013; Karin et al., 2021).

PLAN is a rare neuromuscular degenerative disease caused by mutations in *PLA2G6* gene, located in chromosome 22q13.1, that encodes a calcium-independent Phospholipase A2 group VI enzyme (iPLA2β) (Gregory et al., 2008). More than 200 different mutations in *PLA2G6* have been identified (Hinarejos et al., 2020). PLAN has an autosomal recessive inheritance (Arber et al., 2016; Gregory et al., 2008; Illingworth et al., 2014; Levi and Finazzi, 2014) and it presents three disease phenotypes with different onset age: Infantile Neuroaxonal Dystrophy (INAD), with an early presentation before the first two years of life – the most frequent phenotype (Illingworth et al., 2014) and in which the majority of research works are focused (Iankova et al., 2021) – and Atypical Neuroaxonal Dystrophy (ANAD), with presentation in the early youth (Gregory et al., 2008; Gregory et al., 2009); the third phenotype, *PLA2G6*-related dystonia-parkinsonism, has a late-onset in adulthood (Gregory et al., 2008; Illingworth et al., 2014). Indeed, *PLA2G6* mutations have been proposed as responsible for the PARK14 subtype of Parkinson's Disease (Ferese et al., 2018; Tomiyama et al., 2011; Yoshino et al., 2010; Zhou et al., 2014).

iPLA2β enzyme catalyses the release of fatty acids in *sn2*-position of membrane glycerophospholipids (Arber et al., 2016; Balsinde and Balboa, 2005; Gregory et al., 2008; Gregory et al., 2009). The central role of this enzyme is membrane remodelling by removing peroxidised fatty acids from membranes. In addition, it is involved in cellular signalling because hydrolysed phospholipids release arachidonic acid and lysophospholipids, which acts as signalling molecules (Akiba and Sato, 2004; Arber et al., 2016; Balsinde and Balboa, 2005; Gregory et al., 2008).

The pathological disease process of PLAN has not been completely elucidated (Hayflick et al., 2018; Levi and Finazzi, 2014). Due to the central role of iPLA2β enzyme in membrane remodelling, it has been proposed that impaired membrane lipid homeostasis is the main pathogenic mechanism (Gregory et al., 2008; Gregory et al., 2009; Levi and Finazzi, 2014). These alterations may cause membrane abnormalities (Levi and Finazzi, 2014) and accumulation of oxidized lipids (Arber et al., 2016). As a consequence of membrane composition alterations, oxidative stress and lipid peroxidation could impair autophagy, iron metabolism, mitochondrial function and vesicle-based processes (Arber et al., 2016; Gregory et al., 2009).

There are different experimental models of PLAN, such as the Drosophila iPLA2β mutant strains (Iliadi et al., 2018) and the murine models, principally P*la2g6* knockout (KO) mouse models in which *Beck G., et al 2016* demonstrated the presence of iron accumulation by using Perl's method with diaminobenzidine treatment (Beck et al., 2016). *Pla2g6*-KO mouse lines also revealed mitochondria damage with inner membrane degeneration (Beck et al., 2011; Sumi-Akamaru et al., 2015).

New disease-modifying therapies have been studied and some of them are committed to prevent neurodegeneration by decreasing lipid peroxidation (Hinarejos et al., 2020; Iankova et al., 2021; Kinghorn et al., 2015; Kinghorna and Castillo-Quana, 2016). For example, supplementation with deuterated polyunsaturated fatty acids (D-PUFAs) to reduce lipid peroxidation, or desipramine supplementation, to decrease ceramide accumulation (Iankova et al., 2021). In particular, safety and effectiveness of D-PUFAs has been reported in two cases report (Adams et al., 2020). Currently, there is being conducted a phase II/III clinical trial in 19 INAD patients to study the safety and efficacy of D-PUFAs (Clinical Trials NCT03570931) (Milner, 2018). Unfortunately, to date PLAN therapeutic strategies are mainly symptomatic (Gregory et al., 2008; Hayflick et al., 2018).

Vitamin E, which comprises a family of tocopherols and tocotrienols, has a powerful lipid antioxidant activity that prevents lipid peroxidation (Mustacich et al., 2007). The protective role of vitamin E in the maintenance of neurological health has been established for many years (Ulatowski and Manor, 2015). Furthermore, the potential protective effects of vitamin E supplementation have been suggested in several neurodegenerative diseases, such as Alzheimer's disease or Friedreich's Ataxia, among others (Mustacich et al., 2007; Ulatowski and Manor, 2015). However, further studies are needed to clarify the effectiveness of this drug.

In this work, using two PLAN patients-derived skin fibroblasts cell lines, we evaluated whether cellular models can be a reliable tool for studying PLAN pathophysiology. Although primary skin fibroblasts cultures can be useful research models, they are not the most affected cell type of the disease. For that reason, induced neurons (iNs) were generated from patients-derived PLAN fibroblasts by direct reprogramming (Drouin-Ouellet et al., 2017). Moreover, we assessed the effects of α-tocopherol in correcting the pathophysiological alterations in PLAN cell cultures.

2. Material and methods

2.1. Reagents

Carbonyl Cyanide Chlorophenylhydrazone, α-tocopherol, Luperox® DI, deferiprone, $FeCl_2$, Sudan Black B and Perl's Prussian Blue were purchased from Sigma-Aldrich (Saint Louis, MO, USA). BODIPY® 581/591 C11, MitoTracker™ Deep Red FM, MitoSOX™ Red, MitoTracker™ Red CMXRos, JC-1, Hoechst 3342, DAPI, Anti-Tau clone HT7 antibody were purchased from Invitrogen™/Molecular probes (Eugene, OR, USA). MitoPeDPP® was purchased from Dojindo Molecular Technologies, Inc. (Rockville, MD, USA). S-Bromoenol Lactone was purchased from Cayman Chemical (Ann Arbor, MI, USA). Anti-Actin antibody and Anti-iPLA2β antibody were purchased from Santa Cruz Biotechnology (Dallas, TX, USA).

2.2. Cell cultures and treatments

Two lines of fibroblasts derived from patient skin biopsies, one from an INAD patient and one from an ANAD patient, and two controls lines of primary human skin fibroblasts from healthy volunteers were used. Control and patient fibroblasts were obtained from skin biopsies. Controls were age and sex-matched. Patient 1 (PLAN1) presents a heterozygous mutation c.2221C < T (p.Arg741Trp), that causes a *missense* mutation, and a heterozygous mutation c.2370 T < G (pTyr790Ter), that causes a *nonsense* mutation, which causes a truncated protein (Morgan et al., 2006). Patient 2 (PLAN2) presents a homozygous mutation c.1640A > G (p.Glu547Gly) that causes a *missense* mutation (Cif et al., 2014). Patients and controls samples were obtained according to the Helsinki Declarations of 1964 (revised in 2001). Control values were represented as mean of two control lines. Experiments were performed with less than 12 passage fibroblasts cultures. Patients and controls cultures were maintained in Dulbecco's modified Eagle's medium (DMEM) with Glutamax (Gibco™, ThermoFisher Scientific, Waltham, MA, USA), 100 mg/mL penicillin/streptomycin (Sigma-Aldrich, Saint Louis, MO, USA), and 10% FBS (Gibco™, ThermoFisher Scientific, Waltham, MA, USA). Fibroblasts were cultured at 37 °C and 5% CO_2. iNs were cultured in Neuronal Differentiation medium (NDiff227; Takara-Clontech, Kusatsu, Prefecture of Shiga, Japan) supplemented with neural growth factors and small molecules at different concentrations (Drouin-Ouellet et al., 2017).

Patients and controls fibroblasts were treated with 50 μM of α-tocopherol (named in the text below as vitamin E). Cells were treated for twenty days based on previous studies from our group (Álvarez-Córdoba et al., 2018). As positive control of mitochondrial membrane potential (ΔΨm) depolarization, cell cultures were supplemented for 4 h with 100 μM of Carbonyl Cyanide Chlorophenylhydrazone (CCCP). To induce lipid peroxidation, control cell cultures were treated with 300/500 μM tert-Butylhydroperoxide, Luperox® DI. Other treatments used were 100 μM deferiprone, an iron chelating agent, for 72 h and 100 μM $FeCl_2$ for 2 h, for iron supplementation.

2.3. Cellular morphology analysis

Cellular morphology was analysed by light microscopy images. Areas and perimeters were measure by Fiji-ImageJ software (National Institutes of Health, Bethesda, MD, USA).

2.4. Determination of iron/lipofuscin accumulation

Iron accumulation was determined by Perl's Prussian Blue (PPB) staining (Dang et al., 2010) in fibroblasts and iNs. Images were taken by light and fluorescence Axio Vert A1 microscope (Zeiss, Oberkochen, Germany) with a 20× objective and analysed by Fiji-ImageJ software. Iron levels were also determined by colorimetric Ferrozine-based assay as previously described *Riemer J,* et al. *2004* (Riemer et al., 2004). Moreover, iron content was measured in cell culture extracts by inductively coupled plasma mass spectrometry (ICP-MS) (Tarohda et al., 2005). ICP-MS was performed with an *Agilent* 7800 mass spectrometer (Agilent Technologies, Sana Clara, CA, USA). Extracts were obtained by acid digestion with HNO_3. Lipofuscin accumulation was assessed by Sudan Black B (SBB) staining (Evangelou and Gorgoulis, 2017; Georgakopoulou et al., 2013). SBB stainings were quantified by light microscopy. Autofluorescence was assessed by fluorescence microscopy using an Axio Imager.M2 microscope (Zeiss, Oberkochen, Germany) with a 20× objective. Images were analysed by Fiji-ImageJ software.

2.5. Electron microscopy

Electron microscopy was performed following the protocol previously described by our group (Álvarez-Córdoba et al., 2018; Rodríguez-Hernández et al., 2009). Images were performed on a Libra 120 transmission electron microscope (Zeiss, Oberkochen, Germany).

2.6. Measurement of membrane lipid peroxidation

Lipid peroxidation was evaluated using 4,4-difluoro-5-(4-phenyl-1,3-butadienyl)-4-bora-3a,4a-diaza-s-indacene-3-undecanoic acid (BODIPY® 581/591 C11), a lipophilic fluorescent dye (Alcocer-Gómez et al., 2015; Pap et al., 1999). Cells were incubated with 1–5 μM BODIPY® 581/591 C11 for 30 min at 37 °C. 500 μM Luperox® for 15 min were used as positive control of lipid peroxidation. Lipid peroxidation in fibroblasts was evaluated by an Axio Vert A1 fluorescence microscope with a 20× objective and in iNs using a DeltaVision system (Applied Precision, Issaquah, WA, USA) with an Olympus IX-71 (Olympus®, Shinjuku, Tokio, Japón) fluorescence microscope with a 40× oil objective. Images were analysed with Fiji-ImageJ software.

Mitochondrial lipid peroxidation was evaluated using [3-(4-phenoxyphenylpyrenylphosphino) propyl]triphenylphosphonium iodide (MitoDPPP) fluorescent probe (MitoPeDPP®) developed by *Shioji K., et al 2010* (Shioji et al., 2010). Fibroblasts were treated with 300 nM MitoPeDPP® and 100 nM MitoTracker™ Deep Red FM, an *in vivo* mitochondrial membrane potential-independent probe. Cells' nuclei were stained with 2 μg/mL Hoechst 3342. Positive control of peroxidation was induced using 500 μM Luperox® for 15 min. Images were taken *in vivo* at DeltaVision system with an Olympus IX-71 fluorescence microscope with 40× oil objective and analysed by Fiji-ImageJ software. Colocalization of MitoPeDPP® and MitoTracker™ Deep Red FM was calculated using the DeltaVision system software.

2.7. Measurement of intracellular reactive oxygen species (ROS) generation

Fibroblasts and iNs' mitochondrial superoxide generation was measured using 5 μM MitoSOX™ Red. After staining, cells were analysed by flow cytometry (FACScalibur™ and Cell Quest Pro software, BD Biosciences, San Jose, CA, USA). iNs were stained with 5 μM MitoSOX™ Red and images were taken by a DeltaVision system with an Olympus IX-71 fluorescence microscope with a 40× oil objective. Images were analysed by Fiji-ImageJ software.

2.8. Measurement of mitochondrial membrane potential and mitochondrial morphology determinations

ΔΨm was assessed in fibroblasts and iNs using MitoTracker™ Red CMXRos, a mitochondrial membrane potential-dependent fluorescent dye. Cells were incubated with 100 nM MitoTracker™ Red CMXRos for 45 min at 37 °C. Mitochondrial network was analysed by a semi-automatic morphometric analysis. Parameters as major and minor axis, aspect ratio and percentage of rounded/tubular mitochondria were calculated (Escárcega, 2019; Merrill et al., 2017; Surowka et al., 2014; Yu et al., 2006). We also used JC-1, a mitochondrial membrane potential-dependent probe, which has a fluorescent emission shift from green to red (525 nm/590 nm). Results were expressed as red/green relative ratio. Images were taken by DeltaVision system with an Olympus IX-71 fluorescence microscope with a 40×/60× oil objective and analysed by Fiji-ImageJ software.

2.9. Immunoblotting

Western blotting assays were performed using standard methods. Proteins were transfer to nitrocellulose membrane. Membranes were incubated with primary antibodies at proper dilution range (1:500–1:1000) and, following that, with corresponding secondary antibody coupled to horseradish peroxidase at 1:2500 dilution. Chem-iDoc™ MP Imaging System (Bio-Rad, Hercules, CA, USA) was used to reveal protein signals in membranes. Results were normalized to housekeeping protein actin and they were analysed by ImageLab™ version 5.0 software (Bio-Rad, Hercules, CA, USA).

2.10. Immunofluorescence microscopy

Fibroblasts were plated on glass cover slips (Menzel-Gläser, ThermoFisher Scientific, Waltham, MA, USA) and iNs were seeded on μ-Slide 4 well (Ibidi Inc., Martinsried, Germany). Cells were washed with Phosphate Buffered Saline 1× and fixed with 4% PFA for 10 min. Then, cells were permeabilized with saponin 0,01% or Triton X-100 0,1%, for 10 min. Cells were incubated with blocking solution 5% donkey serum for 1 h. Primary antibodies diluted 1:100–1:200 in blocking solution were incubated overnight at 4 °C. After o/n incubation, cells were washed twice and incubated with secondary antibodies, diluted 1:200 in blocking solution, for 2 h at 37 °C. Finally, cells were stained with 1 μg/mL DAPI for 15–20 min. Cover slides were mounted onto microscope slides using Mowiol® 4–88 (Sigma-Aldrich, Saint Louis, MO, USA). Images were taken with a DeltaVision system with an Olympus IX-71 fluorescence microscope with a 40×/60× oil objective and analysed by Fiji-ImageJ software.

2.11. Cell viability assay

Cell viability was assessed by trypan blue exclusion method (Strober, 2015). Cells were harvested and quantified using trypan blue (Sigma-Aldrich, Saint Louis, MO, USA) by Countess™ 3 Automated Cell Counter

(Invitrogen™, Eugene, OR, USA) at different time points.

2.12. Generation of iNs from PLAN1 fibroblasts by direct reprogramming

Controls and PLAN1 neurons were generated by direct reprogramming (Drouin-Ouellet et al., 2017; Shrigley et al., 2018; Villanueva-Paz et al., 2020; Villanueva-Paz et al., 2019). Fibroblasts were seeded in μ-Slide 4 well or in 24-well plate with 0,1% gelatin-coating. Cells were cultured with DMEM + Glutamax, 100 mg/mL penicillin/streptomycin and 10% of FBS. 24 h later, fibroblasts were infected, with multiplicity of infection of 30, with one-single lentiviral vector, containing two transcription factors (*ASCL1*, *BRN2*) and two shRNA against REST, generated as previously described (Zufferey et al., 1997). Plasmids were obtained as a gift from Malin Parmar (Developmental and Regenerative Neurobiology, Lund University, Sweden). The day after infection, cells medium was replaced with fresh medium. After 48 h, medium was replaced with supplemented NDiff227 as described before (Drouin-Ouellet et al., 2017). Half of medium was changed every 2–3 days. Eighteen days post-infection, medium was replaced with NDiff227 supplemented only with growth factors. Twenty-seven days post-infection, conversion efficiency and neuronal purity were calculated considering Tau+ cells as iNs. Both data were obtained using images from CellDiscoverer7 microscope (Zeiss, Oberkochen, Germany) and analysed images by Fiji-ImageJ software.

2.13. Electrophysiological recordings

Somatic whole-cell patch-clamp recordings were obtained from control iNs in 3 months old cultures. Recordings were performed as previously described (Villanueva-Paz et al., 2020). Briefly, individual coverslips were placed in the recording chamber and perfused at a flow-rate of 3 mL/min with a solution consisting of (in mM): 124 NaCl, 2.69 KCl, 1.25 KH2PO4, 2 $MgSO_4$, 1.8 $CaCl_2$, 26 $NaHCO_3$, and 10 glucose (pH 7.2, 300 mOsm) (bubbled with 95% O_2, 5% CO_2), at RT (22–25 °C). Patch electrodes were made from borosilicate glass and had a resistance of 4–7 MΩ when filled with (in mM): 120 CsCl, 8 NaCl, 1 $MgCl_2$, 0.2 $CaCl_2$, 10 HEPES, 2 EGTA and 20 QX-314 (pH 7.2, 290 mOsm). Current-clamp recordings were performed with a Multiclamp 700B amplifier (Molecular Devices). Data were filtered at 4 kHz, digitized at 10 kHz, and stored in a computer using pClamp software (Molecular Devices, Foster City, CA, USA). This software was used to generate command signals.

2.14. Statistical analysis

Results were expressed as mean ± SD of three independent experiments. Statistical differences were analysed by Student's *t*-test for two groups and ANOVA for more than two groups as parametric statistics methods. In case of using non-parametric methods, we used Mann-Whitney test for two groups and Kruskal-Wallis test to compare multiple groups. Statistically significance was considered by p-values <0.05. Statistical analysis were made with GraphPad Prism 7.0 (GraphPad Software, San Diego, CA USA). Pearson correlation coefficient was calculated with DeltaVision system. A positive correlation was considered when Pearson coefficient > 0.75.

3. Results

3.1. PLAN fibroblasts show iron and lipofuscin accumulation and increased lipid peroxidation

First, we analysed iPLA2β expression levels in fibroblast cell lines derived from two PLAN patients, PLAN1 and PLAN2, and two healthy subjects. PLAN fibroblasts presented reduced protein levels of iPLA2β enzyme in comparison with controls (Fig. 1a, b). Interestingly, PLAN fibroblasts presented an enlarged and flattened cell morphology similar to senescent cells (Fig. S1a-c) (Cho et al., 2004; González-Gualda et al., 2021; Hayflick and Moorhead, 1961; Neurohr et al., 2019). As altered iron metabolism is one of the main characteristics of PLAN mutations, we next examined iron accumulation. PLAN fibroblasts exhibited an increased iron staining compared to controls. As a negative control, PLAN cells were treated with 100 μM deferiprone, an iron-chelating drug, for 72 h (Fig. 1c, d). Iron accumulation in PLAN cells was confirmed by a colorimetric Ferrozine-based assay (Fig. 1e).

As lipofuscin accumulation can result from lipid peroxidation, and it can be also stimulated by iron (Cho and Hwang, 2011; Defendini et al., 1973; Park et al., 1975), we next examined the presence of lipofuscin by autofluorescence analysis, SBB staining and electron microscopy in control and PLAN fibroblasts.

Lipofuscin granules presents a fluorescence emission spectrum between 500 and 640 nm (Cho and Hwang, 2011). PLAN fibroblasts showed an increase autofluorescence compared to controls (Fig. 1f, g). Since the presence of metals (iron, copper…) has been described in lipofuscin (Cho and Hwang, 2011), we assessed the presence of iron in lipofuscin treating the cells with 100 μM deferiprone for 72 h. A reduction of autofluorescence in PLAN fibroblasts was showed (Fig. S1d, e) suggesting the presence of iron in form of lipofuscin. PLAN cells stained with SBB also showed an augmentation of stained lipofuscin compared to controls (Fig. 1h, i). Furthermore, lipofuscin granules differences were also evident in electron microscopy observations (Fig. 2).

As PLAN mutation affects the renewal of membrane lipids, we next assessed the presence of lipid peroxidation in cell membranes by BODIPY™ staining. Results showed increased levels of lipid peroxidation in PLAN fibroblasts relative to control ones (Fig. 3).

3.2. Relationship between lipid peroxidation and iron accumulation

Literature supports the evidence of the relation between iron, ROS production and lipid peroxidation (Frolova et al., 2015; Höhn and Grune, 2013; Rockfield et al., 2018; Zhao et al., 2021). As consequence of increase intracellular iron, the Fenton reaction occurs and generates high levels of ROS, which damage lipids through peroxidation (Rockfield et al., 2018). With the aim to know whether lipid peroxidation, as the primary event, may be involved in the iron accumulation process, we treated healthy fibroblasts for 2 h with 500 μM Luperox® to induce lipid peroxidation and with 100 μM $FeCl_2$ as a positive control of iron overload. As shown in Fig. 4, peroxidation induced by Luperox® led to an increase in iron accumulation. Moreover, cells acquired a senescent-like morphology. To confirm induced-iron accumulation by lipid peroxidation, we measured iron content by Ferrozine assay (Fig. 4e) and iron levels were significantly increased in cells treated with Luperox® and $FeCl_2$. Furthermore, we also assessed the presence of lipofuscin granules under Luperox-induced lipid peroxidation conditions. Therefore, both Luperox-induced peroxidation and iron overload elicited an increment of lipofuscin accumulation (Fig. S2).

Moreover, iPLA2β enzyme was inhibited by S-Bromoenol Lactone ((*S*)-BEL), a specific irreversible inhibitor of the enzyme, in a control cell line; the results showed that lack of enzyme function produced an increase in the levels of lipid peroxidation and iron accumulation (from 10 μM of (*S*)-BEL) after 24 h of incubation (Fig. S3 and S4).

3.3. Vitamin E treatment reverts cell morphology, iron and lipofuscin accumulation in PLAN fibroblasts

Next, we evaluated the effect of vitamin E treatment, a well-known membrane antioxidant, on iron accumulation. After screenings with different concentrations, 50 μM vitamin E was the lowest concentration able to remove iron accumulation (Fig. 5a). Vitamin E treatment reduced significantly iron overload in PLAN fibroblasts (Fig. 5b, c), assessed by PPB staining, and reverted their senescent morphology (Fig. 6a, b). Reduction of iron levels by vitamin E treatment was also confirmed by ICP-MS and Ferrozine assays (Fig. 5d, e). Moreover,

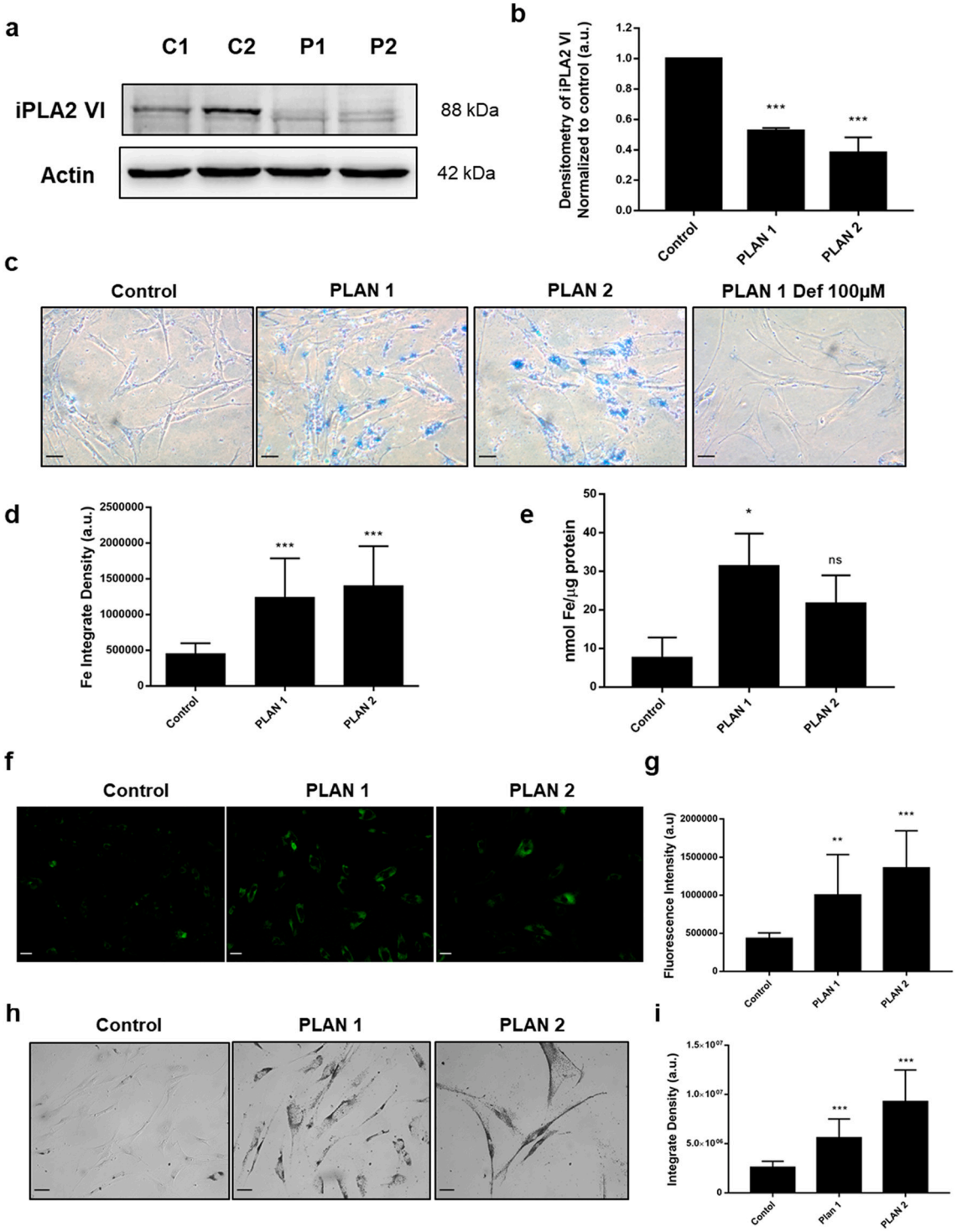

Fig. 1. Pathophysiological characterization of PLAN fibroblasts cell lines. (a) iPLA2β protein expression levels analysed by Western blotting of two PLAN fibroblasts and two healthy subjects. Actin was used as a loading control. (b) Densitometry of Western blotting, control reflects the values of C1 and C2. (c) Representative images of iron accumulation assessed by PPB staining in two PLAN fibroblasts lines and one PLAN line treated with 100 μM deferiprone (Def) for 72 h as a negative control. Scale bar = 50 μm. (d) Iron staining quantification. (e) Iron accumulation determined by colorimetric Ferrozine-based assay. (f) Representative images of lipofuscin autofluorescence. Scale bar = 50 μm. (g) Quantification of autofluorescence. (h) Representative images of lipofuscin staining by SBB. Scale bar = 50 μm. (i) Lipofuscin staining quantification. Data represent the mean ± SD of three separate experiments (at least 30 images for each condition and experiment were analysed). Significance between PLAN and control fibroblasts is represented as ***p-value <0.001, **p-value <0.01, *p-value <0.05. Significance between deferiprone treated and untreated lines is represented as [a]p-value <0.001, [b]p-value <0.01, [c]p-value <0.05.

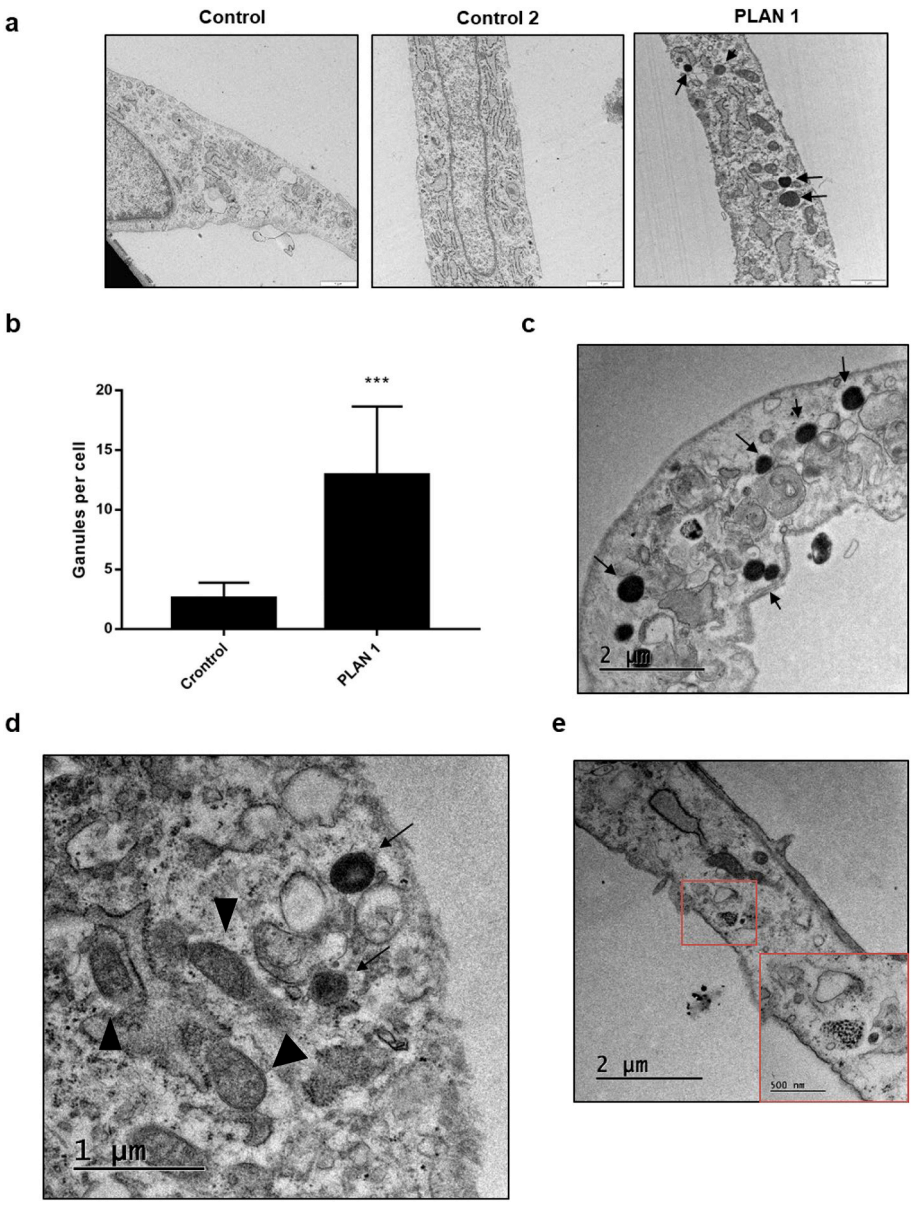

Fig. 2. (a) Representative images from electron microscopy of control and PLAN fibroblasts. Scale bar = 1 µm. (b) Quantification of lipofuscin granules. (c) Detail of lipofuscin granules in PLAN1 fibroblasts cell line. (d, e) Detail of degenerated internal mitochondria cristae. Arrows point to lipofuscin granules; head arrows point to mitochondria. Significance between PLAN and control fibroblasts is represented as ***p-value <0.001.

treated PLAN fibroblasts evidenced a significant reduction in SBB staining and lipofuscin autofluorescence intensity compared with untreated cells (Fig. 6c-f). The positive effects of vitamin E on the elimination of iron and lipofuscin accumulation were not due to changes in iPLA2β protein expression levels, which remained low under vitamin E supplementation (Fig. 7). This fact rules out the possibility that the positive effect of vitamin E would be ascribed to an increase of residual mutant enzyme as occurs in PKAN mutations after pantothenate supplementation (Álvarez-Córdoba et al., 2018).

3.4. Vitamin E treatment reduces oxidative stress and lipid peroxidation in PLAN fibroblasts

Lipid peroxidation in PLAN fibroblasts was significantly reduced under vitamin E treatment (Fig. 8). Furthermore, vitamin E treatment prevented superoxide accumulation in PLAN cells (Fig. S5a). In addition, vitamin E treatment was able to improve PLAN cell viability in presence of 300 µM Luperox® (Fig. S5b). Specifically, increased levels of mitochondrial lipid peroxidation were showed in PLAN fibroblasts compared to controls. As expected, Vitamin E treatment significantly reduced mitochondrial lipid peroxidation (Fig. 9a, b). Co-localization analysis corroborated the specific presence of peroxidation in mitochondria (Fig. 9c, d).

3.5. Vitamin E treatment improves mitochondrial dysfunction and mitochondrial network morphology

PLAN patients-derived fibroblasts showed a reduction in ΔΨm associated with increased mitochondrial network fragmentation (Fig. 10). Interestingly, vitamin E treatment improved both ΔΨm and mitochondrial network (Fig. 11). To confirm these results, we also assessed ΔΨm by JC-1 staining (Fig. S6).

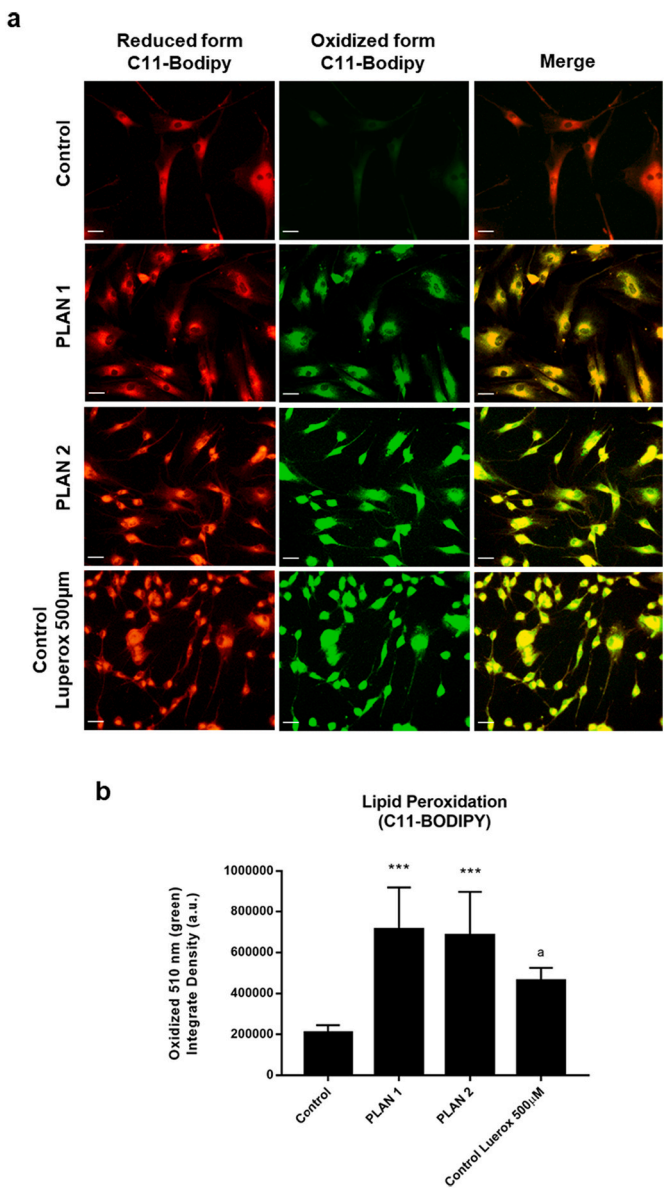

Fig. 3. (a) Representative images of lipid peroxidation in control and PLAN fibroblasts by BODIPY® 581/591 C11 staining. Positive control of peroxidation was included treating control fibroblasts with Luperox® (500 μM, 15 min). Scale bar = 50 μm. (b) Fluorescence quantification. Data represent the mean ± SD of three separate experiments (at least 30 images for each condition and experiment were analysed). Significance between PLAN and control fibroblasts is represented as ***p-value <0.001. Significance between Luperox® treated and untreated control lines is represented as [a]p-value <0.001.

3.6. Evaluation of the positive effects of vitamin E supplementation on iNs derived from PLAN fibroblasts

Patient-derived PLAN1 fibroblasts and control fibroblasts were transdifferentiated into iNs by transducing lentiviral vectors containing proneural genes (Drouin-Ouellet et al., 2017; Villanueva-Paz et al., 2020; Villanueva-Paz et al., 2019). Twenty-seven days post-infection, cells presented neuron-like morphology and positive immunoreactivity against Tau (Fig. 12a, b). We used Tau+ cells to evaluate neuronal conversion efficiency and results showed a percentage around 20%. Neuronal purity was around 90% (Fig. 12c, d). Neuronal electrophysiological properties were detected in generated iNs. The resting membrane potentials (RMP) of neuron-like cells were − 23.9 ± 1.3 mV from Control iNs. A step protocol that fixes the membrane potential of the cell at different values shows that 4% of Control iNs generate action potentials. Moreover, spontaneous activity (sEPSCs) was also observed (Fig. 12e).

PLAN1 iNs showed an increased iron staining and superoxide production compared to controls (Fig. 13a-d). PLAN1 iNs also presented a higher area and perimeter of neuronal soma than control iNs (Fig. 13e, f).

Vitamin E treatment in PLAN1 iNs showed a positive effect of attenuating iron accumulation (Fig. 14a, b) and reducing significantly neuronal soma area and perimeter (Fig. 14c, d). Vitamin E treatment also reduced superoxide production in PLAN1 iNs in comparison with untreated PLAN1 iNs (Fig. 15). As expected, PLAN1 iNs showed an increase in peroxidised lipids compared to control iNs. Furthermore, vitamin E treatment of PLAN iNs induced a statistically significant reduction in lipid peroxidation (Fig. 16). Finally, vitamin E treatment also significantly improved ΔΨm of PLAN1 iNs (Fig. 17).

4. Discussion

In this study, we have assessed the pathophysiology of two patients-derived fibroblasts lines with *PLA2G6* mutations. We propose that skin fibroblasts, obtained from patients' dermal biopsies, and iNs, obtained by direct reprograming, harbouring the own patients' mutations, are suitable biological models that recreate the pathophysiology of the disease. As an advantage, the combination of cellular models and high throughput screening also offers the possibility of evaluating the effect of large numbers of potential drugs for PLAN treatment.

One common characteristic of NBIA disorders is brain iron accumulation. As shown in other NBIA subtypes, iron accumulation and impaired iron metabolism have been previously reported in different PKAN and BPAN fibroblasts and neuronal models (Álvarez-Córdoba et al., 2018; Aring et al., 2020; Campanella et al., 2012; Ingrassia et al., 2017; Santambrogio et al., 2015). In PLAN, iron accumulation was previously described in a iPLA2β KO mouse model (Beck et al., 2016).

In this work, we show that iron accumulation can be detected in both PLAN cellular models, fibroblasts and iNs. Interestingly, we demonstrate that iron overload is accompanied by the presence of lipofuscin granules. Lipofuscin accumulation is associated with aging and neurodegeneration, and it has been observed in Parkinson's and Alzheimer's diseases (Moreno-García et al., 2018). In addition, lipofuscin accumulation has been described by our research group in cells derived from PKAN patients (Álvarez-Córdoba et al., 2018). As the exposition of PLAN fibroblasts to an iron-chelator drug led to a reduction of lipofuscin autofluorescence, our results suggest a close relationship between both processes, lipofuscin formation and iron recruitment.

Lipid peroxidation is developed by two mechanisms, enzyme-mediated processes and non-enzymatically spontaneous autoxidation. In non-enzyme mediated processes, the interaction between H_2O_2 and free ferrous iron generates hydroxyl radicals, which mediates the initiation step of lipid peroxidation. In the propagation phase, lipid radicals react with oxygen to form lipid peroxyl radicals and lipid hydroperoxides (Yin et al., 2011).

Lipid peroxidation plays a central role in PLAN pathogenesis (Kinghorn et al., 2015) and it has been described as the main consequence of *PLA2G6* mutations (Arber et al., 2016). PLAN fibroblasts and iNs showed increased levels of peroxidised lipids, as observed by other studies. For instance, *Kinghorn KJ., et al 2015* described increased lipid peroxidation in iPLA2-*VIA*$^{-/-}$ flies and fibroblasts derived from a patient with *PLA2G6* mutation (homozygous p-R747W) (Kinghorn et al., 2015).

PLA2G6 gene is ubiquitously expressed, having a relevant role in the central nervous system (Balboa et al., 2002). iPLA2β resides in the cytosol, but its translocation to membrane compartments was documented in response to stress, especially to the mitochondria (Aoun and Tiranti, 2015). Mitochondria are the energy factory of eukaryotic cells. Mitochondrial activity is especially important in neurons that have an elevated energy consumption for synaptic dynamics and

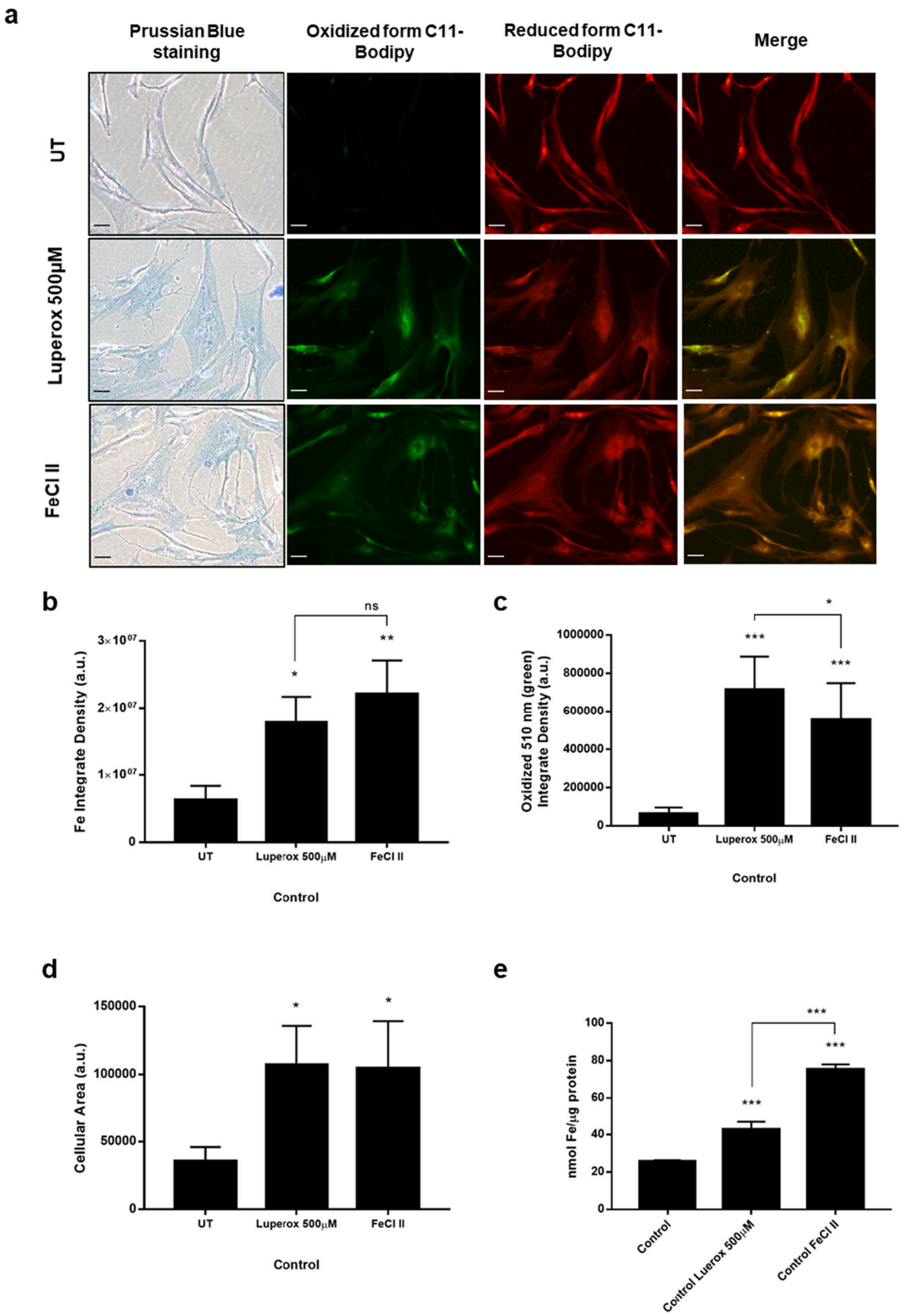

Fig. 4. Effect of lipid peroxidation on iron accumulation. (a) Control fibroblasts were treated for 2 h with Luperox® (500 μM) and FeCl2 (100 μM). Lipid peroxidation was determined by BODIPY® 581/591 C11staining and iron accumulation by PPB staining. Scale bar = 50 μm. (b) Quantification of iron staining. (c) Quantification of fluorescence of Oxidized (510 nm) form of C11-Bodipy. (d) Quantification of cellular area. (e) Iron levels determined by colorimetric Ferrozine-based assay. Data represent the mean ± SD of three separate experiments (at least 30 images for each condition and experiment were analysed). Significance is represented as ***p-value <0.001, **p-value <0.01, *p-value <0.05.*3.3.*

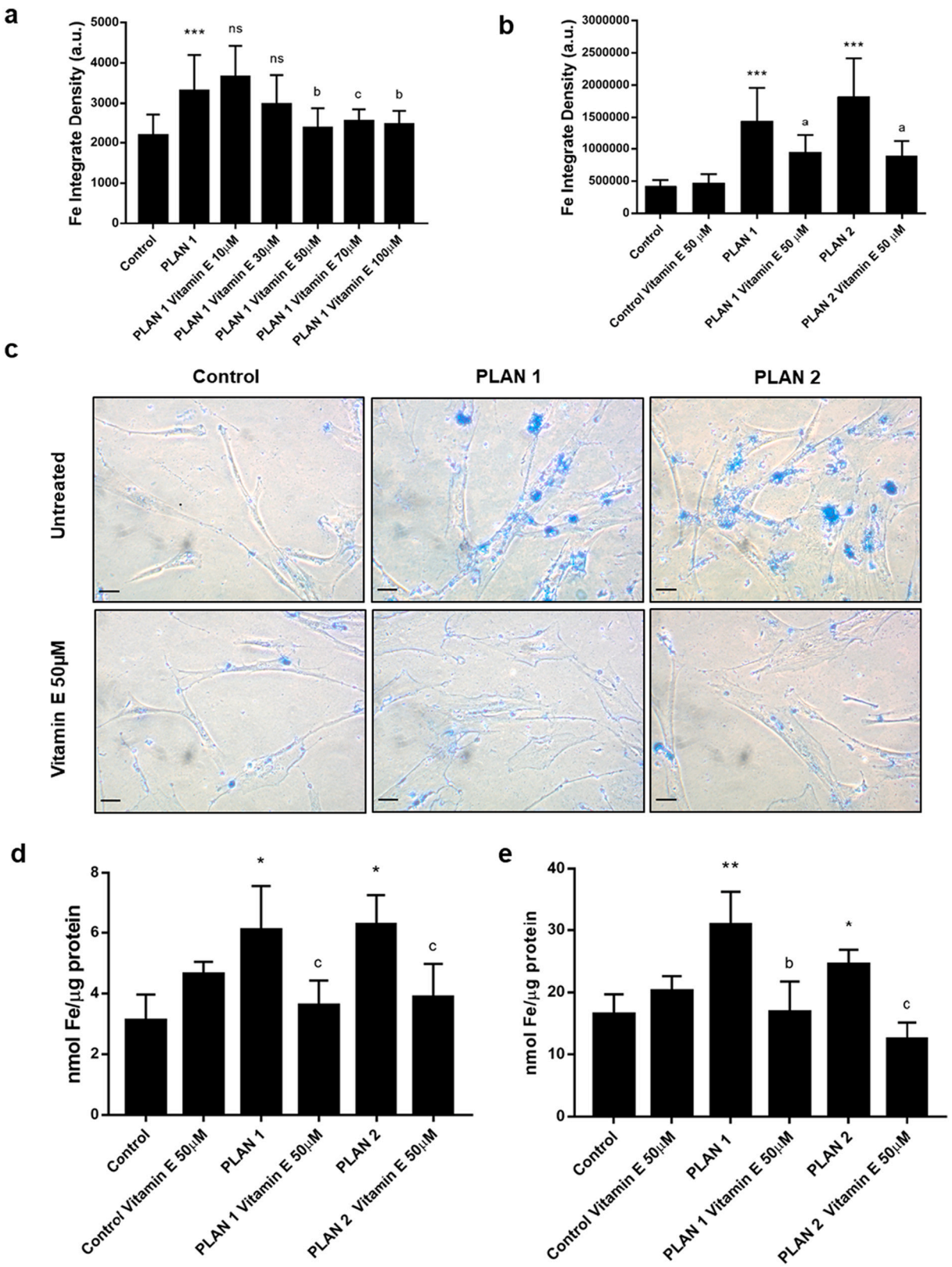

Fig. 5. Effect of vitamin E (50 μM) supplementation for twenty days on iron accumulation in PLAN fibroblasts. (a) Iron quantification by PPB staining of PLAN fibroblasts treated with vitamin E (10, 30, 50, 70 and 100 μM). (b) Iron staining quantification in control and PLAN fibroblasts untreated and treated with 50 μM vitamin E. (c) Representative images of iron staining by PPB. Scale bar = 50 μm. (d) Iron levels in control and PLAN fibroblasts untreated and treated with 50 μM vitamin E by ICP-MS. (e) Iron levels in control and PLAN fibroblasts untreated and treated with 50 μM vitamin E by colorimetric Ferrozine-based assay. Data represent the mean ± SD of three separate experiments (at least 30 images for each condition and experiment were analysed). Significance between PLAN and control fibroblasts is represented as ***p-value <0.001, **p-value <0.01, *p-value <0.05. Significance between vitamin E (50 μM) treated and untreated lines is represented as [a]p-value <0.001, [b]p-value <0.01, [c]p-value <0.05.

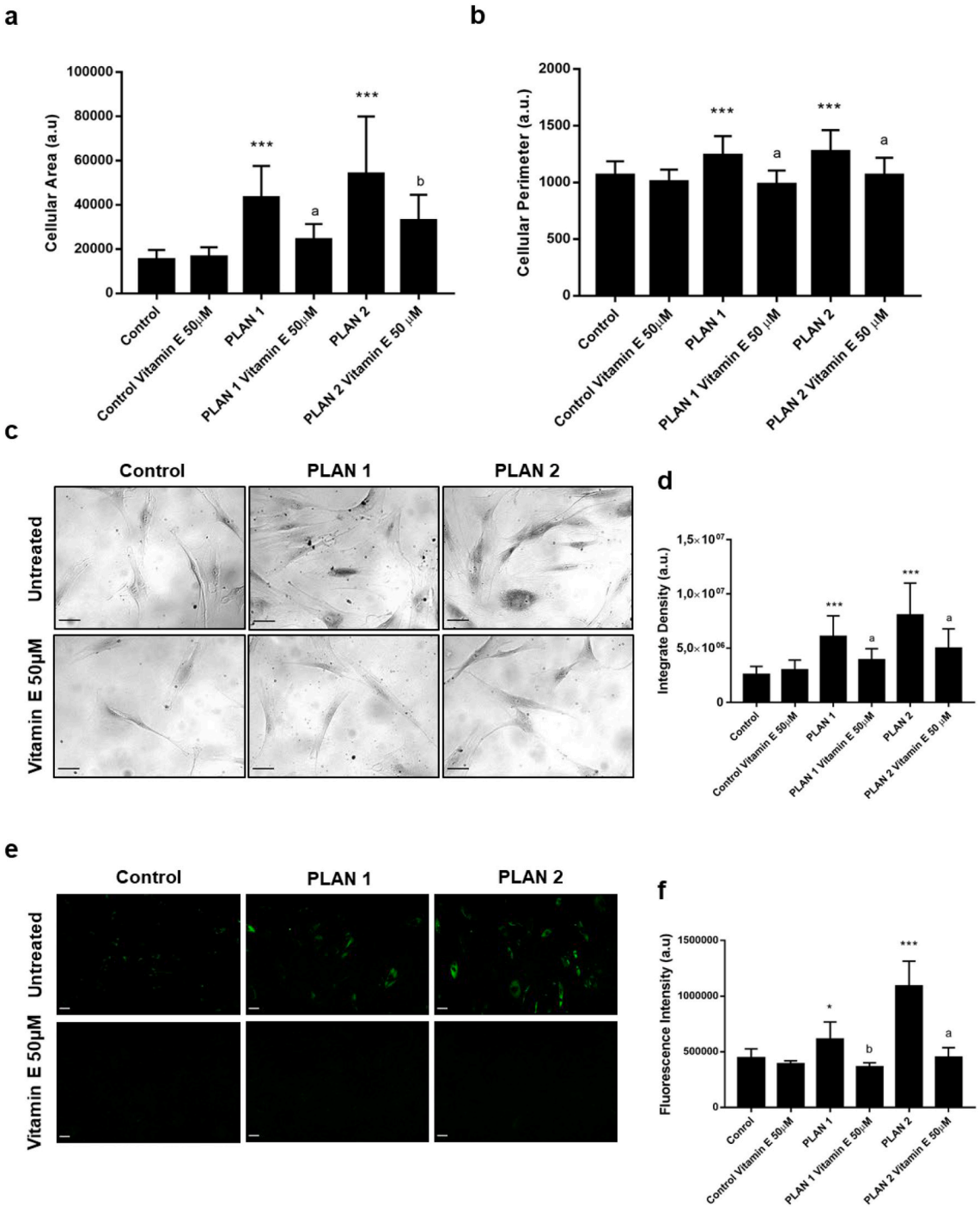

Fig. 6. Effect of vitamin E (50 μM) on cell morphology and lipofuscin content. (a) Quantification of cellular area and (b) cellular perimeter. (c) Representative images of lipofuscin staining by SBB of untreated and treated control and PLAN fibroblasts. Scale bar = 50 μm. (d) SBB staining quantification. (e) Representative images of untreated and treated control and PLAN fibroblasts autofluorescence. Scale bar = 50 μm. (f) Autofluorescence quantification. Data represent the mean ± SD of three separate experiments (at least 30 images for each condition and experiment were analysed). Significance between PLAN and control fibroblasts is represented as ***p-value <0.001, **p-value <0.01, *p-value <0.05. Significance between vitamin E (50 μM) treated and untreated lines is represented as [a]p-value <0.001, [b]p-value <0.01, [c]p-value <0.05.

neurotransmitter production. As a consequence of mitochondrial activity, large amounts of ROS are generated (Hinarejos et al., 2020). Multiple studies demonstrated that iPLA2β expression prevents ROS accumulation and loss of ΔΨm in response to stress-induced apoptosis (Ching-Chi et al., 2017; Hinarejos et al., 2020; Seleznev et al., 2006). In our work, we observed high levels of ROS in both *PLA2G6* mutant fibroblasts and iNs. As inner mitochondria membrane is highly sensible to ROS due to its high cardiolipin content (Hinarejos et al., 2020), we assessed if mitochondria could be also affected by lipid peroxidation. A significant increase of mitochondrial lipid peroxidation was detected in mutant PLAN fibroblasts. These findings are in agreement with previous studies reporting that the loss of iPLA2β activity was associated with structural abnormalities of mitochondrial membrane with inner mitochondria membrane degeneration (Beck et al., 2011; Kinghorn et al., 2015; Sumi-Akamaru et al., 2015). Abnormal respiration and low ΔΨm, related with excessive ROS production were observed in animal PLAN

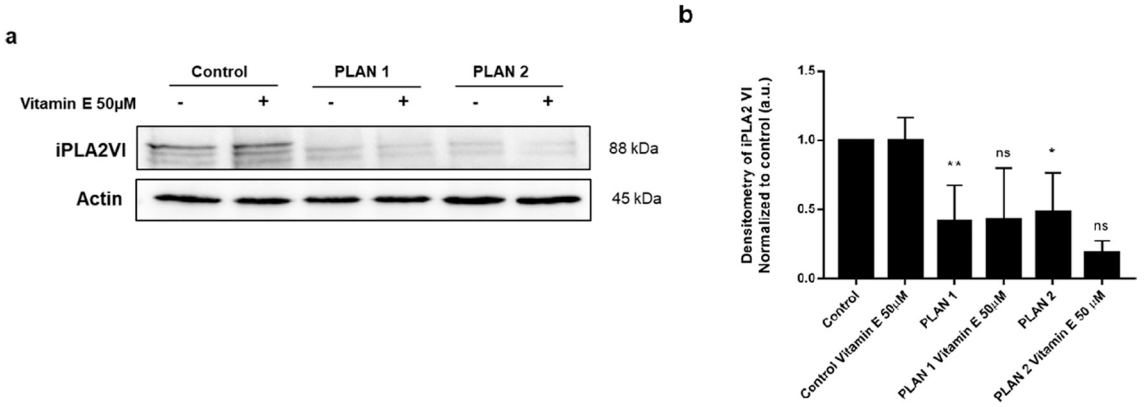

Fig. 7. Effect of vitamin E treatment (50 μM) on iPLA2β protein levels. (a) Representative image of iPLA2β protein levels analysed by Western blotting of treated and untreated control and PLAN fibroblasts and (b) Densitometry of Western blotting. Data represent the mean ± SD of three separate experiments. Significance between PLAN and control fibroblasts is represented as ***p-value <0.001, **p-value <0.01. Significance between vitamin E treated and untreated lines is represented as [a]p-value <0.001.

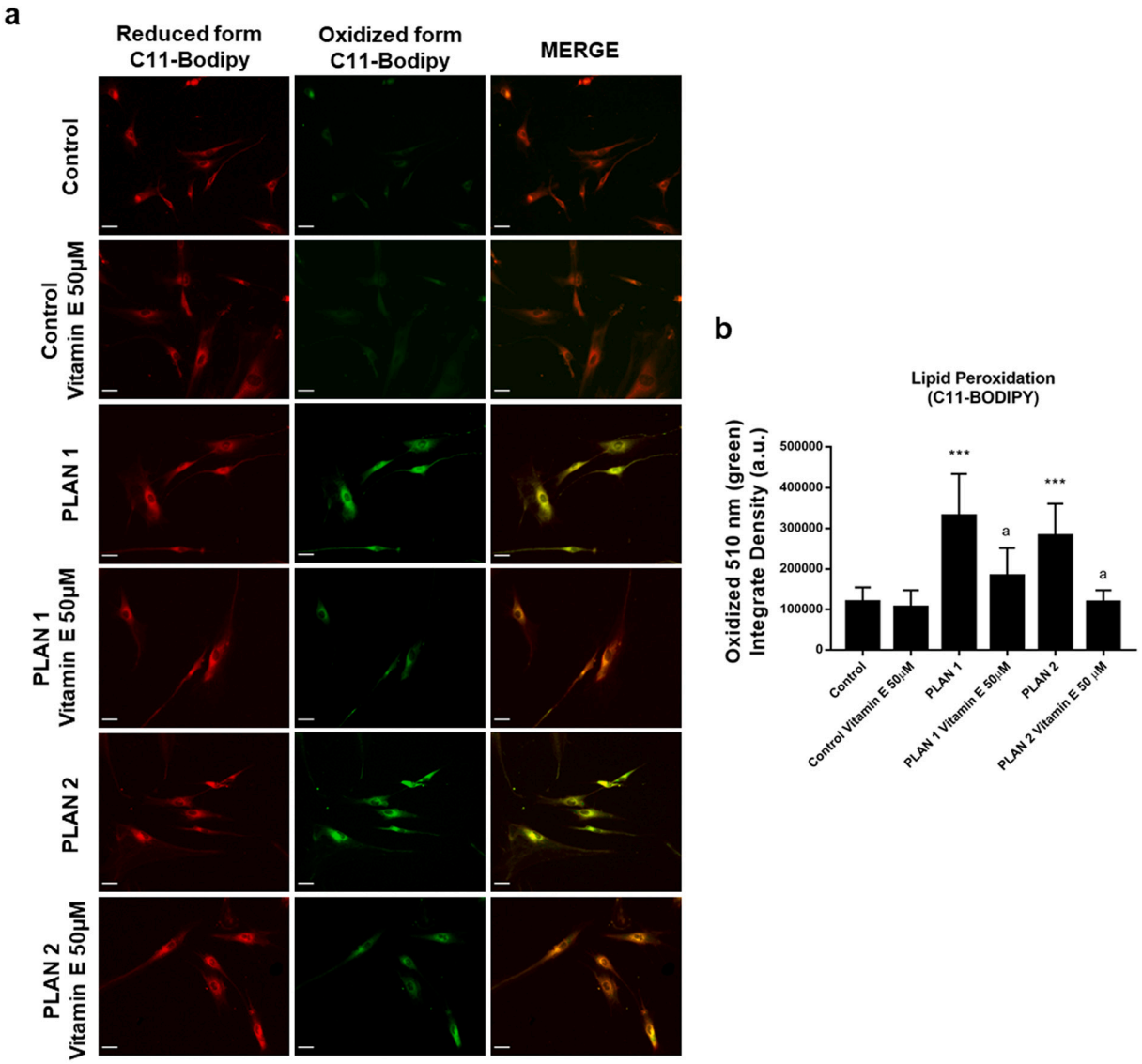

Fig. 8. Effect of vitamin E (50 μM) treatment on lipid peroxidation. (a) Representative images of lipid peroxidation in treated and untreated control and PLAN fibroblasts by BODIPY® 581/591 C11 staining. Scale bar = 50 μm. (b) Fluorescence quantification of Oxidized (510 nm) form of C11-Bodipy. Data represent the mean ± SD of three separate experiments (at least 30 images for each condition and experiment were analysed). Significance between PLAN and control fibroblasts is represented as ***p-value <0.001. Significance between vitamin E (50 μM) treated and untreated lines is represented as [a]p-value <0.001.

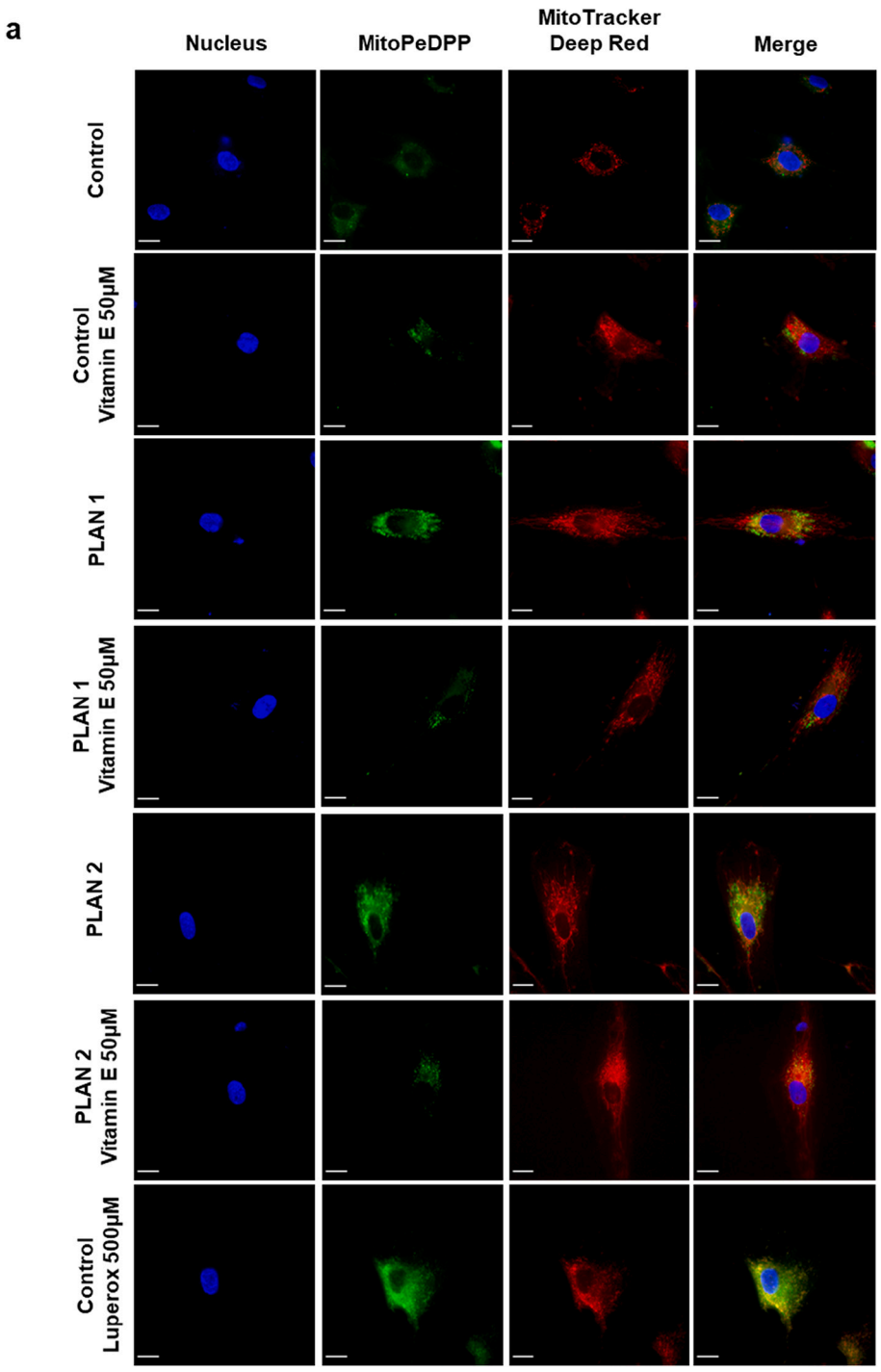

Fig. 9. Effect of 50 μM vitamin E treatment on mitochondrial lipid peroxidation. (a) Representative images of mitochondrial lipid peroxidation in treated and untreated control and PLAN cells. Control cells treated with Luperox® (500 μM) for 15 min were used as a positive control of mitochondrial lipid peroxidation. Scale bar = 20 μm. (b) Quantification of MitoPeDPP® fluorescence. (c) To corroborate the specific MitoPeDPP® presence in the mitochondrion, cells were also stained with MitoTrackerTM Deep Red FM and calculated the Pearson correlation coefficient, scale bar = 20 μm, and (d) the number of co-localized puncta per cell of both probes. Positive correlation was considered with a Pearson coefficient > 0.75. PLAN fibroblast present a Pearson coefficient above 0.8, as well as Luperox® treated control. Data represent the mean ± SD of three separate experiments (at least 30 images for each condition and experiment were analysed). Significance between PLAN and control fibroblasts is represented as ***p-value <0.001, **p-value <0.01. Significance between vitamin E (50 μM) treated and untreated lines is represented as ^{b}p-value <0.01, ^{c}p-value <0.05. Significance between Luperox® treated healthy fibroblasts and untreated is represented as $^{\#}$p-value <0.001. (For interpretation of the references to colour in this figure legend, the reader is referred to the web version of this article.)

models (Kinghorn et al., 2015). We evaluated ΔΨm and mitochondrial network in *PLA2G6* mutant fibroblasts and results showed a significant reduction in ΔΨm, as well as mitochondrial network disruption with reduced mitochondrial elongation and increased number of rounded depolarized mitochondria. Reduced ΔΨm was also observed in PLAN iNs. Our findings in both PLAN models reinforce previous studies in which a significant decrease of ΔΨm has been described in fibroblasts derived from a patient with *PLA2G6* mutation (homozygous p-R747W),

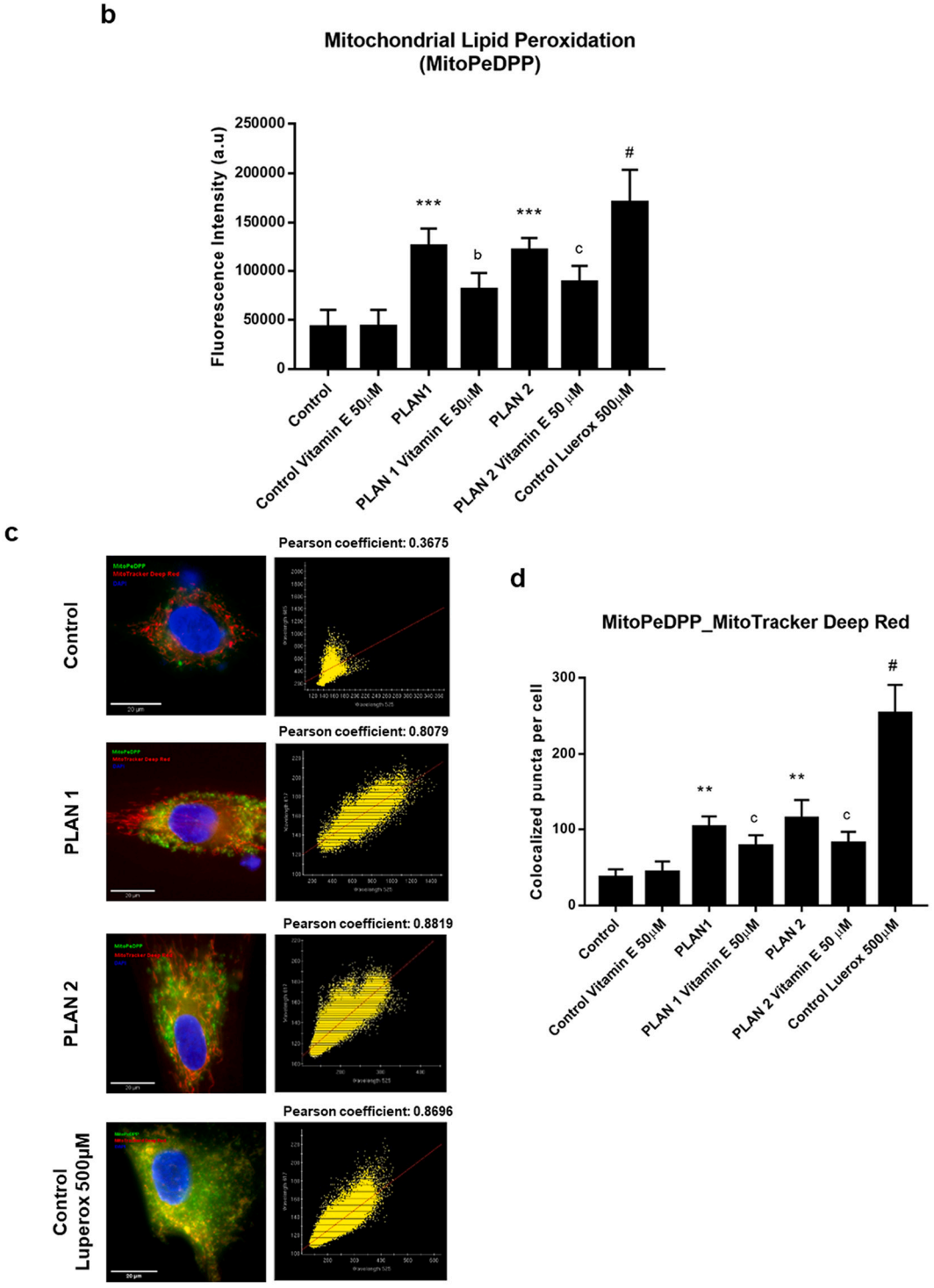

Fig. 9. (*continued*).

as well as iPLA2-*VIA*$^{-/-}$ fly brains (Kinghorn et al., 2015).

In order to elucidate the role of lipid peroxidation in iron accumulation, we assessed the effect of Luperox® induced-peroxidation on control fibroblasts. Treatment of control fibroblasts with Luperox® increased lipid peroxidation, iron accumulation and led to senescent-like morphological changes, exhibiting a phenotype similar to mutant PLAN fibroblasts. The supplementation of control cells with $FeCl_2$ also induced iron overload and lipid peroxidation. These results suggest that lipid peroxidation *per se* induces iron accumulation, and that iron accumulation induces lipid peroxidation in a vicious cycle. Previously, it has been described that iron contributes to lipid peroxidation as it occurs in pathological changes of age-related macular degeneration (Zhao et al., 2021). Excess of iron produces ROS through Fenton reaction and it is involved in primary and secondary products of lipid peroxidation formation such as hydroperoxyl lipids (Rockfield et al., 2018; Zhao et al., 2021).

On the other hand, we showed that the treatment with Luperox® and $FeCl_2$ induced lipofuscin accumulation in healthy cells. Stress conditions lead to accumulation of oxidized lipids, proteins aggregates and lipofuscin and lipid peroxidation has been associated with lipofuscin

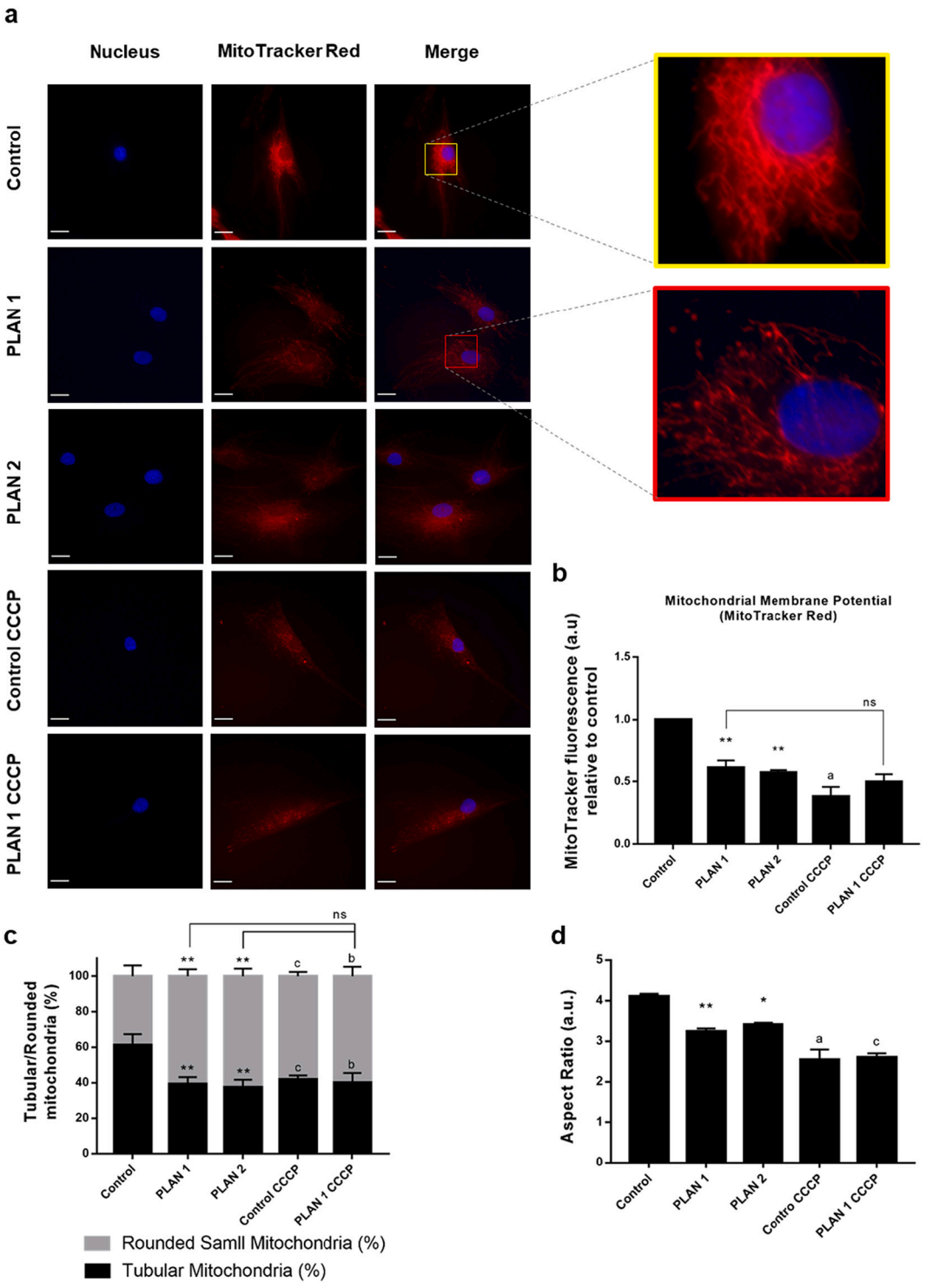

Fig. 10. Characterization of ΔΨm and mitochondrial network of PLAN fibroblasts lines. (a) Representative images of control and PLAN fibroblasts stained with MitoTrackerTM Red CMXRos. As a positive control of membrane depolarization, we used 100 μM CCCP for 4 h in controls. Scale bar = 20 μm. (b) Fluorescence quantification. (c) Quantification of tubular and rounded percentage of mitochondria in control and PLAN fibroblasts. (d) Quantification of Aspect Ratio. Data represent the mean ± SD of three separate experiments (at least 30 images for each condition and experiment were analysed). Significance between PLAN and control fibroblasts is represented as ***p-value <0.001, **p-value <0.01. Significance between CCCP treated and untreated lines is represented as [a]p-value <0.001, [b]p-value <0.01, [c]p-value <0.05. (For interpretation of the references to colour in this figure legend, the reader is referred to the web version of this article.)

formation (Cho and Hwang, 2011; Krohne et al., 2010; Moreno-García et al., 2018). Lipofuscin, that is described to be composed by oxidized lipids and proteins in a not degradable and insoluble form, is not only a consequence of oxidative stress; it has an active role in free radicals formation and consequent cytotoxicity (Höhn and Grune, 2013; Moreno-García et al., 2018). Lipofuscin presents redox activity and it is able to recruit iron in a redox-active manner and to catalyse the Fenton reaction on its surface (Höhn and Grune, 2013). Moreover, proteasome inhibition has been described as a consequence of lipofuscin accumulation (Moreno-García et al., 2018; Powell et al., 2005; Sitte et al., 2000).

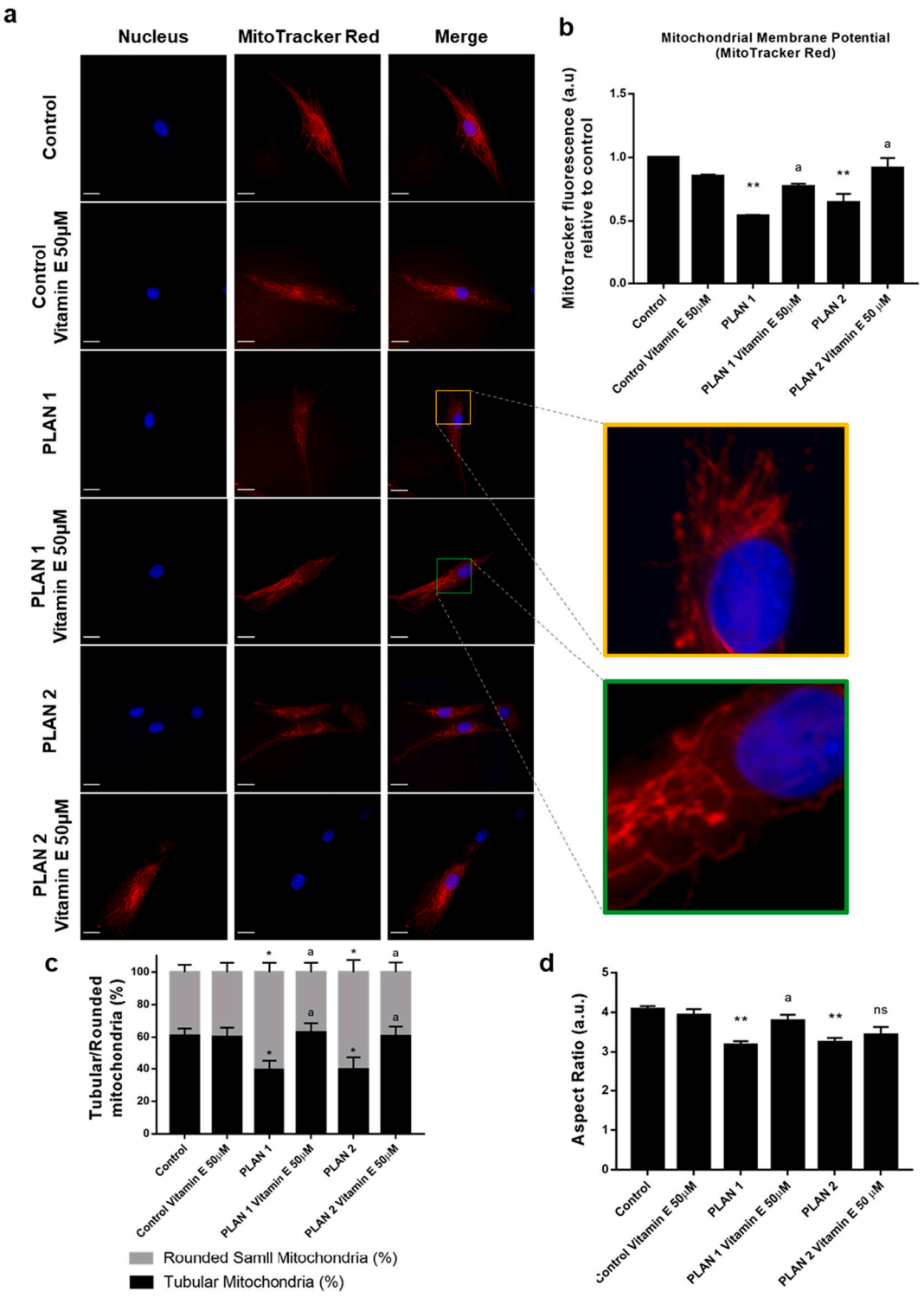

Fig. 11. Effect of vitamin E (50 μM) treatment on ΔΨm and mitochondrial network. (a) Representative images of vitamin E (50 μM) treated and untreated of control and PLAN fibroblasts stained with MitoTrackerTM Red CMXRos. Scale bar = 20 μm. (b) Quantification of fluorescence. (c) Quantification of tubular and rounded mitochondria. Rounded mitochondria were defined as 0,2–0,9 μm and tubular mitochondria as >0,9 μm. (d) Quantification of Aspect Ratio. Aspect Ratio was calculated as major/minor axis and has a minimum value of 1 that correspond with perfect circle, their value increase as mitochondrial network elongates. Data represent the mean ± SD of three separate experiments (at least 30 images for each condition and experiment were analysed). Significance between PLAN and control fibroblasts is represented as ***p-value <0.001, **p-value <0.01. Significance between vitamin E (50 μM) treated and untreated lines is represented as [a]p-value <0.001, [b]p-value <0.01, [c]p-value <0.05. (For interpretation of the references to colour in this figure legend, the reader is referred to the web version of this article.)

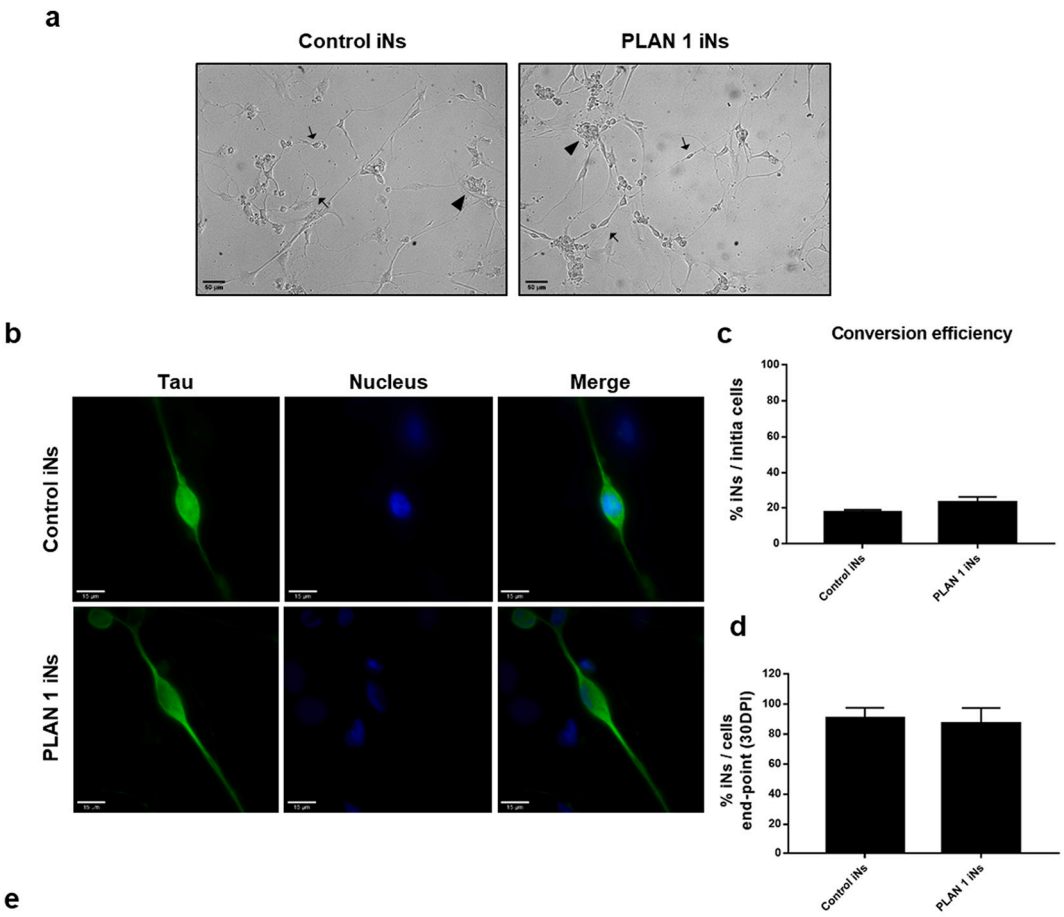

	Control iNs
RMP (mV)	23.9 ± 1.3
Rin (MΩ)	1763 ± 242.1
τ (ms)	41.7 ± 9
Proportion of spiking cells	1/25
Threshold (mV)	-33
Amplitude (mV)	36.5
Widhs (ms)	280
Frequency sEPSP (Hz)	2.14 ± 0.65
Amplitude sEPSP (mV)	0.62 ± 0.05

Fig. 12. Characterization of PLAN generated iNs. (a) Representative images of control and PLAN iNs at 27 days post-infection by bright-field microscopy. Arrows point to cells with iNs morphology; Head arrows point to iNs-like cells clusters. Scale bar = 50 μm. (b) Representative images of iNs stained with Tau, a microtubule-associated protein main located in neuronal axons of vertebrate brain. Undifferentiated cells showed only nuclear staining. Scale bar = 15 μm. (c) Conversion efficiency, the number of Tau+ cells over the total fibroblasts seeded at the beginning of reprogramming. (d) Neuronal purity, the number of Tau+ cells over the total cells in the plate after reprograming. (e) Electrophysiological properties of cultured cells (3 months) control iNs by whole-cell recordings. Rin, Inward resistance; T, time constant.

There are different hypothesis that can explain lipofuscin formation. Lysosomal dysfunction has been hypothesised to play a role in lipofuscin formation by the accumulation of lipofuscin in lysosomes due to an impaired macroautophagy (Höhn and Grune, 2013; Milward et al., 2012). Iron also plays a role in development of lipofuscin formation though the lysosomes aggregation. Thus, intralysosomal iron may catalyse the Fenton reaction producing hydroxyl radicals, which cause lipid and protein oxidation within the lysosome. Damaged secondary lysosomes can fuse with other lysosomes and the endogenous material aggregates, leading to lipofuscin accumulation (Milward et al., 2012). Other hypothesis suggests the mitochondrial origin of lipofuscin. Previous research describes how lipofuscin formation occurs in isolated mitochondria, due to increased lipid peroxidation caused by mitochondrial iron (Frolova et al., 2015). In addition, both lipofuscin formation pathways seem to be related. The hypothesis of Terman and Brunk, referred to as the "mitochondrial-lysosomal axis theory of aging", assumes that the incomplete degradation of damaged mitochondria, mediated by autophagy, is the cause for lipofuscin accumulation (Brunk and Terman, 2002). Although it has not been clearly experimentally proven, some results found in the literature support this hypothesis. While dysfunctional mitochondria degradation by autophagy is a rapid process in young healthy cells, in senescent cells, reduced autophagy or insufficient lysosome activity trigger mitochondrial damage and lipofuscin accumulation. Hydrogen peroxide is able to diffuse into

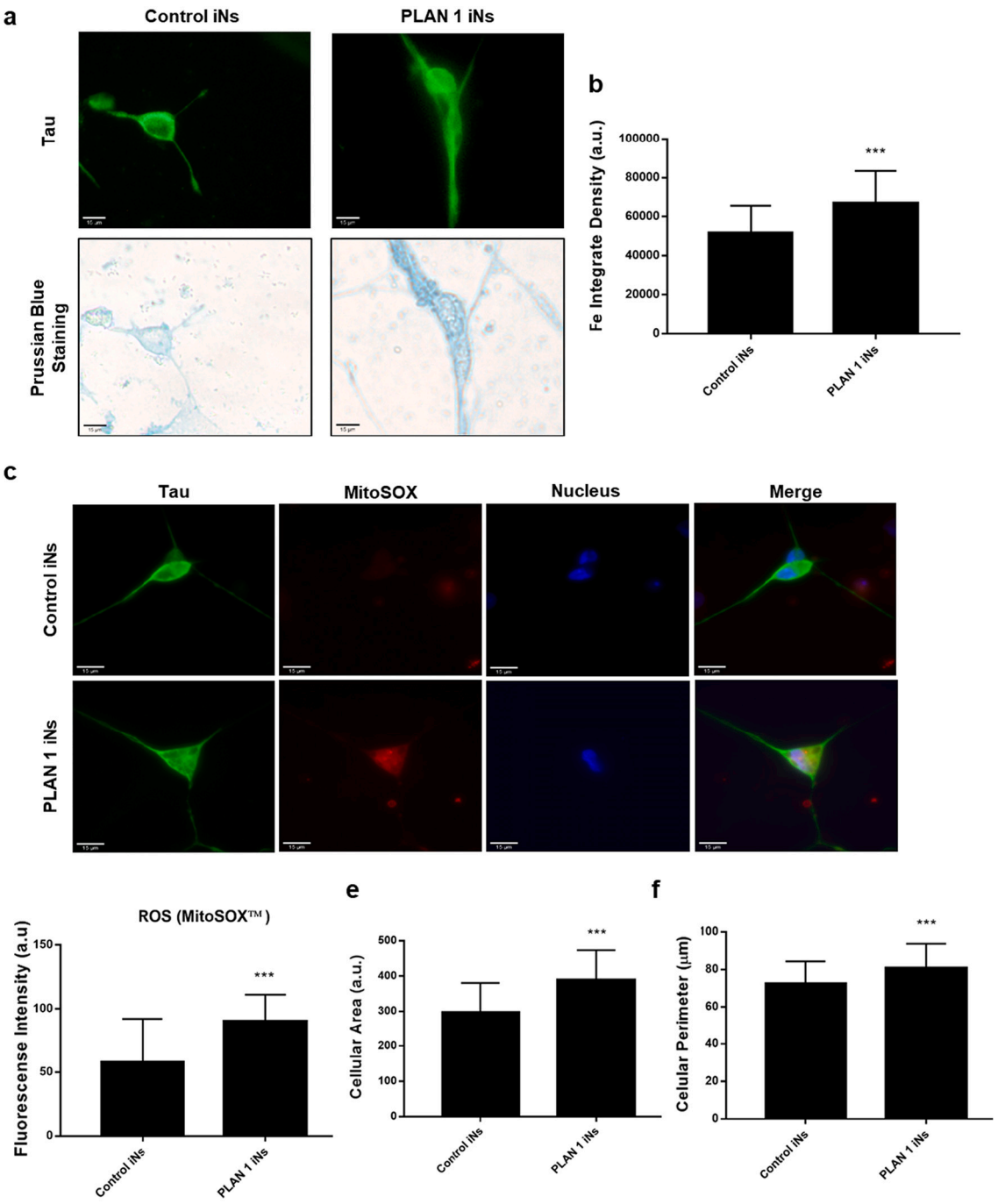

Fig. 13. Pathophysiological characterization of PLAN1 iNs. (a) Representative images of iron accumulation by PPB staining in Tau+ cells. Scale bar = 15 µm. (b) Quantification of iron staining in control and PLAN1 iNs. (c) Representative images of ROS production in Tau+ cells by MitoSOXTM Red. Scale bar = 15 µm. (d) Fluorescence quantification. (e) Quantification of neuronal soma area and (f) perimeter. Data represent the mean ± SD of three separate experiments (at least 30 images for each condition and experiment were analysed). Significance between PLAN1 and control iNs is represented as ***p-value <0.001. (For interpretation of the references to colour in this figure legend, the reader is referred to the web version of this article.)

lysosomes and reacts with iron producing a gradual accumulation of non-degradable lipofuscin (Frolova et al., 2015; Kurz et al., 2008; Moreno-García et al., 2018).

We hypothesize that the induction of mitochondrial lipid peroxidation *per se* may induce iron accumulation in the form of lipofuscin. Therefore, a possible pathogenic mechanism in PLAN might be that lipid peroxidation occurs progressively due to the lack of iPLA2β activity and that mitochondrial lipid peroxidation is aggravated and propagated by the presence of high concentration of iron in mitochondria. Previous studies (Beck et al., 2011; Kinghorn et al., 2015; Kinghorna and Castillo-Quana, 2016; Sumi-Akamaru et al., 2015) and our findings in PLAN fibroblasts and iNs such as lipid peroxidation, mitochondrial dysfunction and excessive ROS production support this hypothesis. Interestingly, mitochondria with disruption of the internal mitochondrial cristae were observed by electron microscopy in PLAN fibroblasts (Supplementary Fig. 2d, e), similar to those described by *Beck G., et al 2011* (Beck et al., 2011). On the other hand, other studies suggest alteration of autophagy and vesicle-based processes as part of pathophysiology of PLAN (Arber et al., 2016; Davids et al., 2016; de-Figueiredo, de Figueiredo et al., 2000; Gregory et al., 2009). All these mechanisms are interconnected

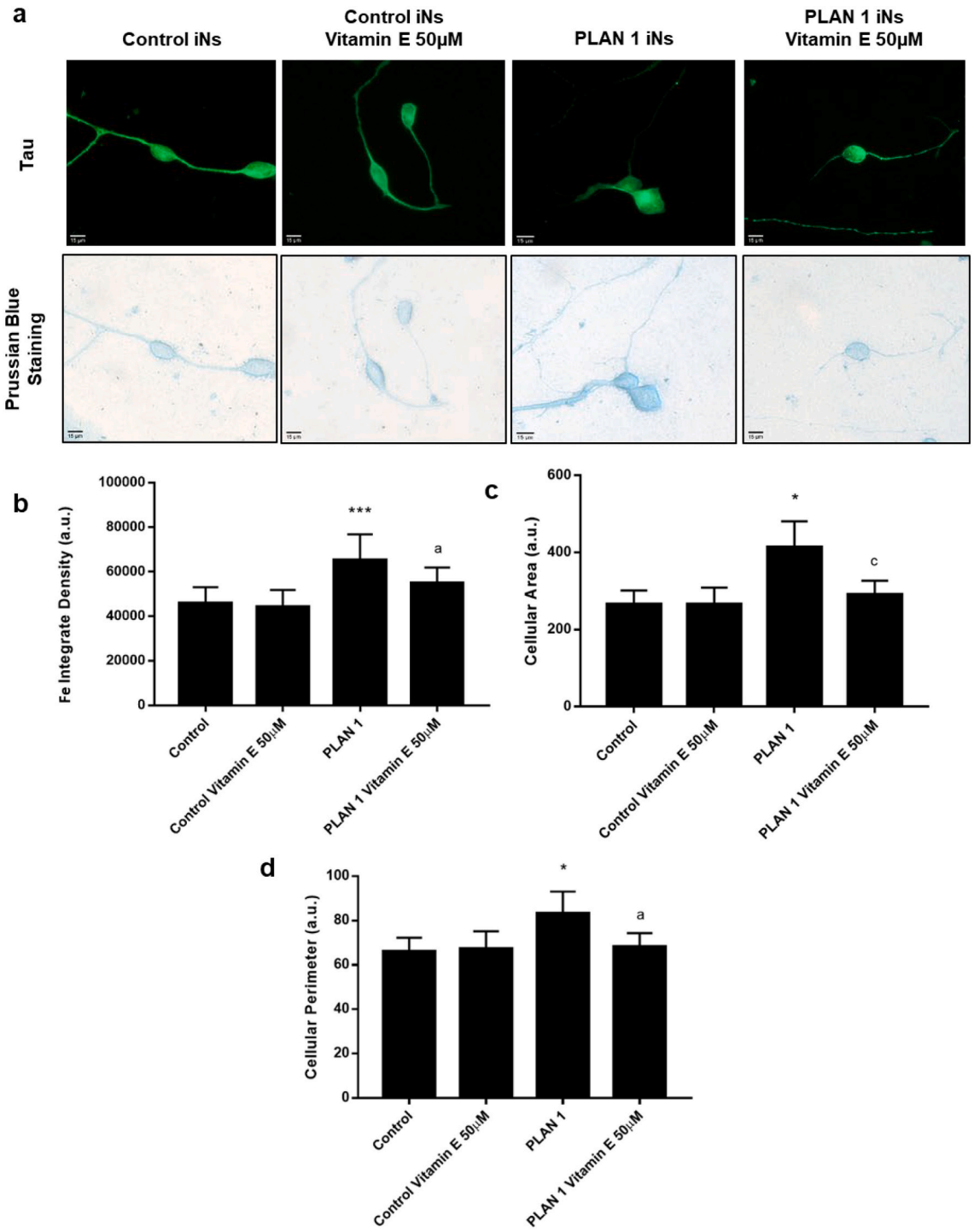

Fig. 14. Effect of vitamin E (50 μM) treatment on iron accumulation in PLAN1 iNs. (a) Representative images of iron accumulation by PPB staining in vitamin E (50 μM) treated and untreated control and PLAN1 iNs. Scale bar = 15 μm. (b) Quantification of iron levels by PPB staining in vitamin E (50 μM) treated and untreated control and PLAN1 iNs. (c) Neuronal soma area and (d) perimeter quantification of control and PLAN1 iNs with and without vitamin E (50 μM) treatment. Data represent the mean ± SD of three separate experiments (at least 30 images for each condition and experiment were analysed). Significance between PLAN1 and control iNs is represented as ***p-value <0.001, *p-value <0.05. Significance between vitamin E (50 μM) treated and untreated lines is represented as [a]p-value <0.001, [c]p-value <0.05.

and may participate in lipofuscin formation. Moreover, a similar mechanism of lipofuscin accumulation has been proposed by our group in patients-derived PKAN fibroblasts (Álvarez-Córdoba et al., 2018). However, the origin of iron accumulation and lipofuscin formation needs further study.

Our results are in disagreement those from *Guo YP.,* et al. *2019*, who found that iPLA2β activity inhibition by (*S*)-bromoenol lactone led to no obvious iron accumulation. The authors concluded that iPLA2β or *PLA2G6* gene deficiency is not the possible cause for iron accumulation *in vitro*. To explain this controversy some considerations must be take into account. First, lipid peroxidation was not determined after iPLA2β inhibition; and second, the exposition of cells to the inhibitor was only

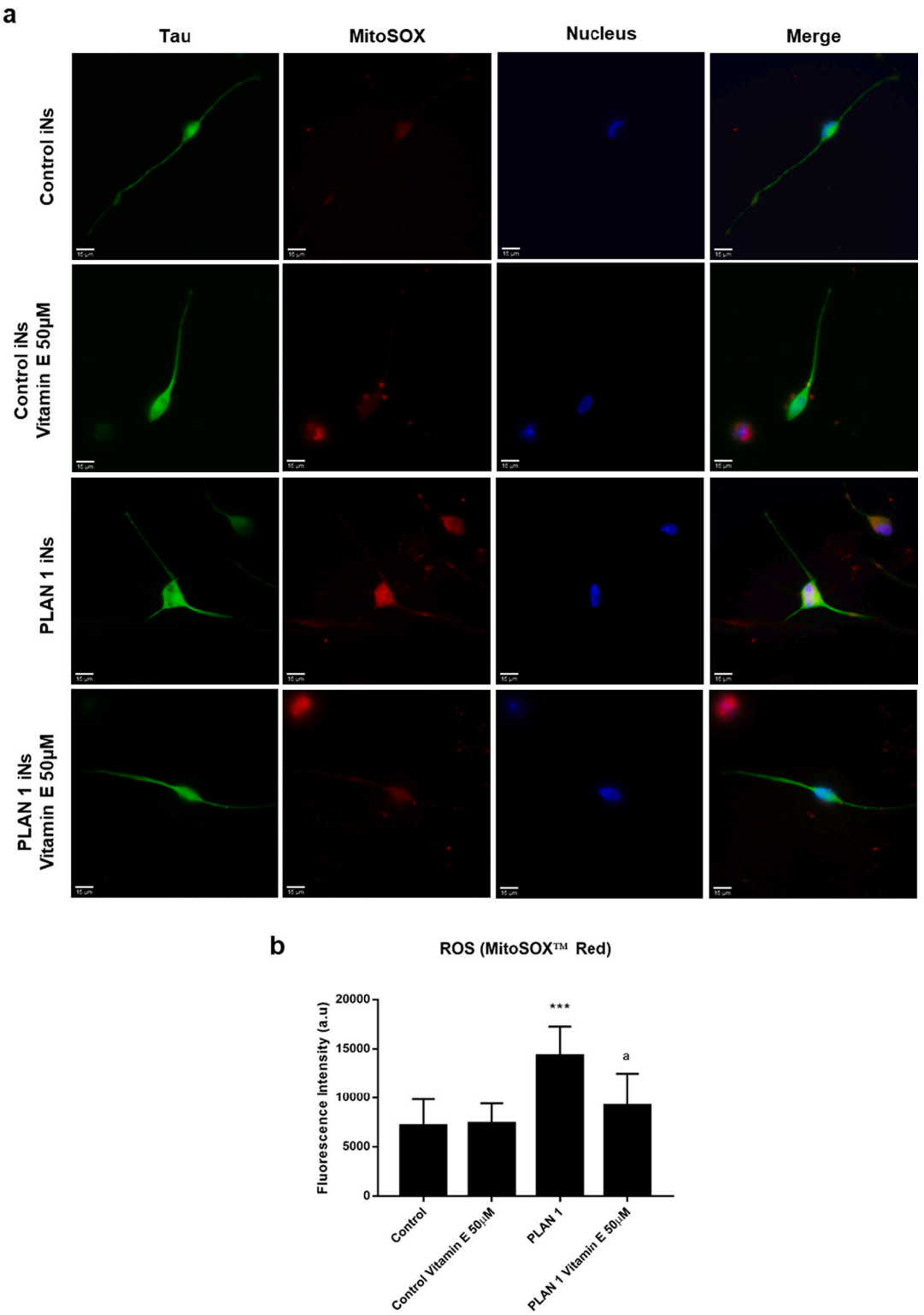

Fig. 15. Effect of vitamin E treatment (50 μM) on ROS production in PLAN1 iNs. (a) Representative images of ROS production by MitoSOX™ Red in vitamin E (50 μM) treated and untreated control and PLAN1 iNs. Scale bar = 15 μm. (b) Fluorescence quantification. Data represent the mean ± SD of three separate experiments (at least 30 images for each condition and experiment were analysed). Significance between PLAN1 and control iNs is represented as ***p-value <0.001. Significance between vitamin E (50 μM) treated and untreated lines is represented as [a]p-value <0.001. (For interpretation of the references to colour in this figure legend, the reader is referred to the web version of this article.)

30 min. (Guo et al., 2019). The dose-dependent increase of cell death in these experimental conditions could be explained by the non-specific effect of the drug on cell viability.

In previous investigations, the use of a lyophilic antioxidant in *PLA2G6* mutants fibroblasts revealed a reduction in lipid peroxidation and ΔΨm improvement (Kinghorna and Castillo-Quana, 2016). The use of early antioxidant and anti-inflammatory therapies would help to attenuate the progression of the disease in patients (Hinarejos et al.,

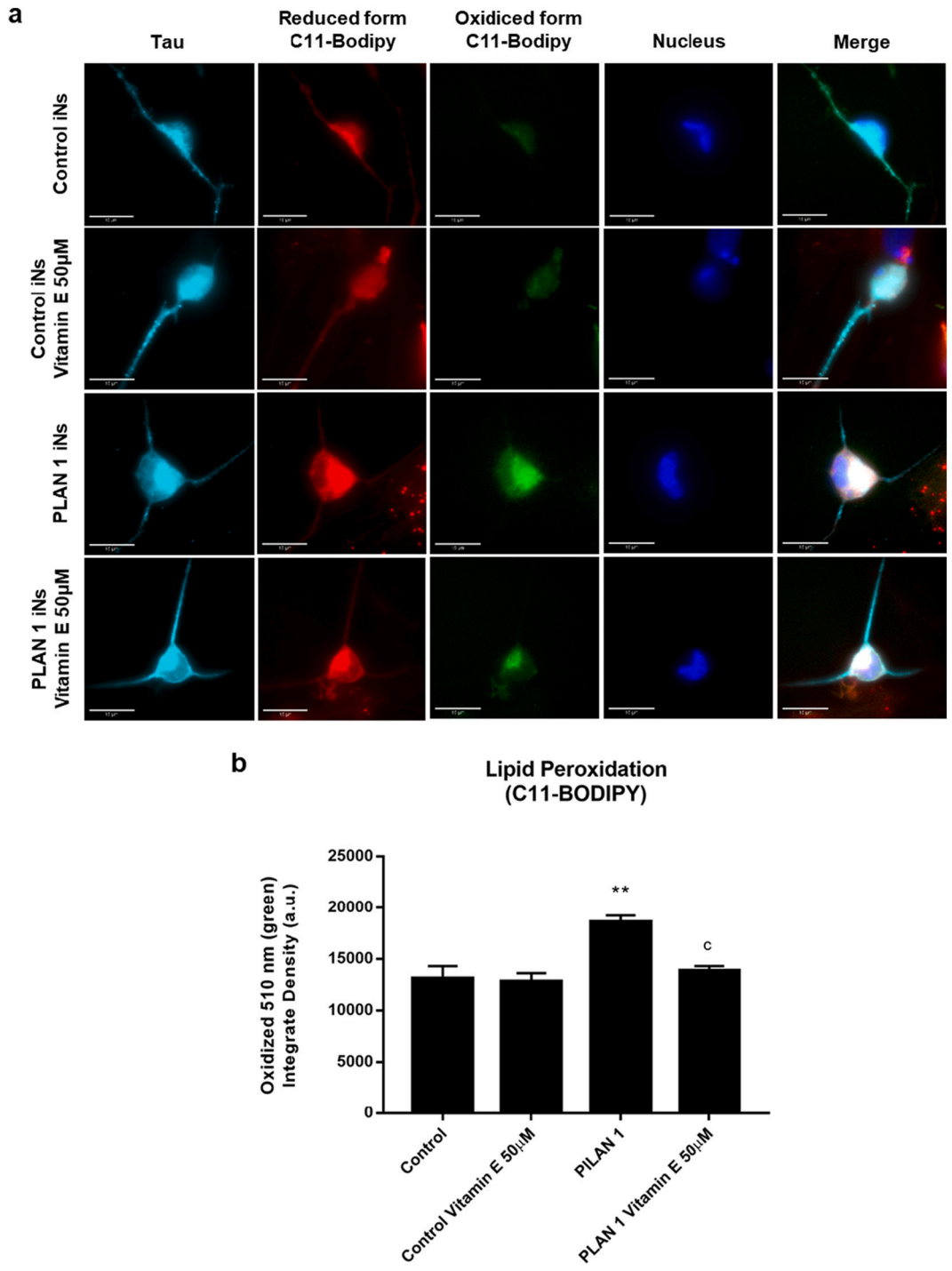

Fig. 16. Effect of vitamin E (50 μM) treatment on lipid peroxidation in PLAN1 iNs. (a) Representative images of lipid peroxidation in vitamin E (50 μM) treated and untreated control and PLAN1 iNs by BODIPY® 581/591 C11 staining. Scale bar = 15 μm. (b) Fluorescence quantification of Oxidized (510 nm) form of C11-Bodipy. Data represent the mean ± SD of three separate experiments (at least 30 images for each condition and experiment were analysed). Significance between PLAN1 and control iNs is represented as **p-value <0.01. Significance between vitamin E (50 μM) treated and untreated lines is represented as ^{c}p-value <0.05.

2020; Kinghorna and Castillo-Quana, 2016). Vitamin E has been studied as a potential treatment in other neurodegenerative diseases associated with mitochondrial dysfunction, oxidative stress and lipid peroxidation, such as Huntington's, Alzheimer's or Parkinson's diseases (Butterfield et al., 2002; Johri and Beal, 2012). In the present work, we used vitamin E for its antioxidant capacity and, especially, for its protective effect on lipid peroxidation (Niki, 2014). In PLAN fibroblasts, vitamin E treatment improved cell viability under the exposition of lipid peroxidation agents and induced a reduction in lipid peroxidation, ROS production and iron accumulation. Previous research reported the positive effect of vitamin E on mitochondrial superoxide generation acting as biological modifier, independently of its antioxidant capacity (Chow, 2001). In PLAN iNs, vitamin E treatment was also able to improve the pathological alterations. Positive effects of vitamin E treatment are probably due to its capability of block the spread of peroxidation by donating a hydrogen atom to the lipid peroxyl radical species (Niki, 2014; Yin et al., 2011). This characteristic makes vitamin E an efficient ferroptosis inhibitor. Ferroptosis is a type of cell death caused by the accumulation of iron-

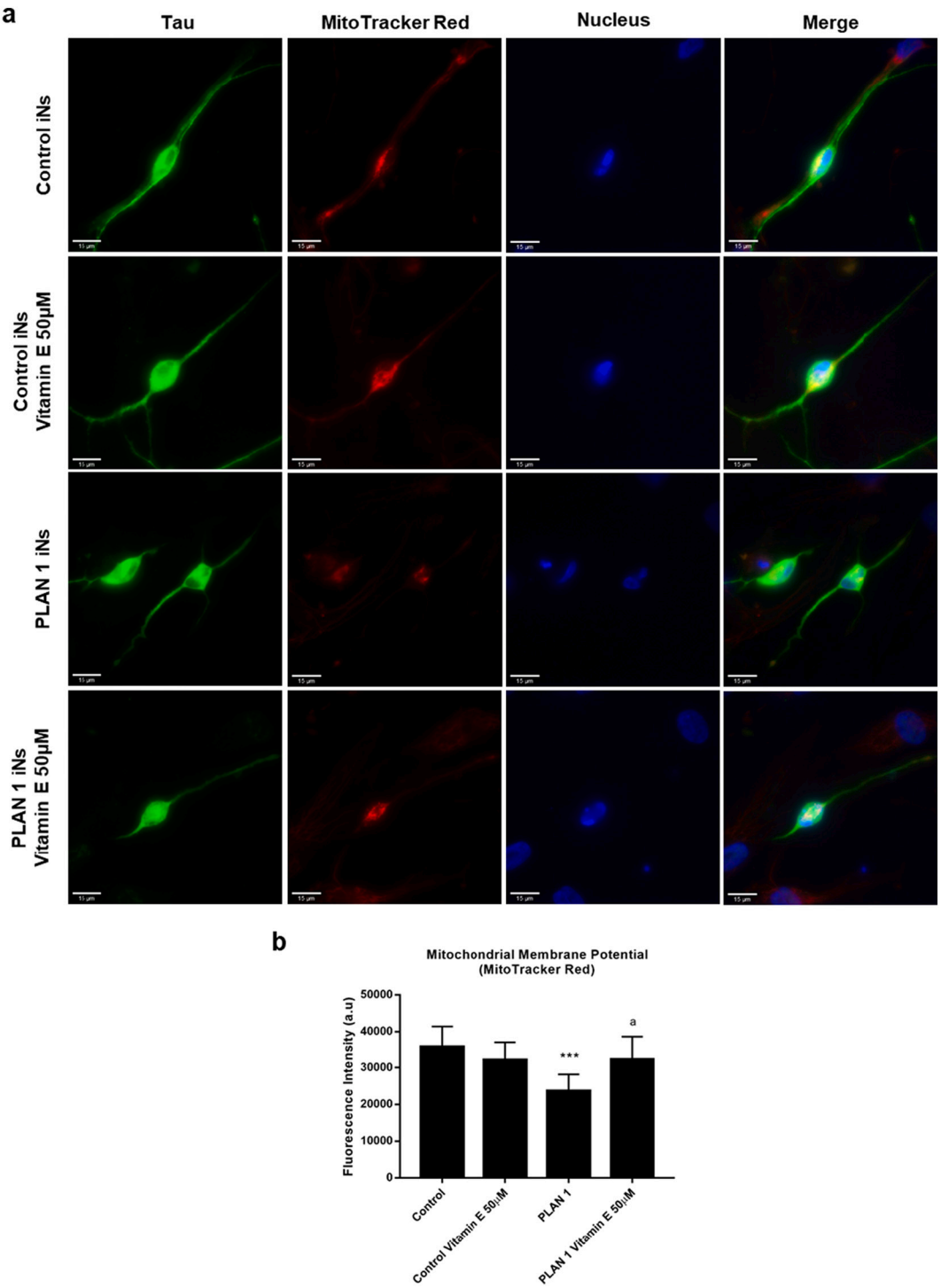

Fig. 17. Effect of vitamin E (50 μM) treatment on ΔΨm in PLAN1 iNs. (a) Representative images of vitamin E (50 μM) treated and untreated control and PLAN1 iNs stained with MitoTrackerTM Red CMXRos fluorescence dye. Scale bar = 15 μm. (b) Quantification of fluorescence. Data represent the mean ± SD of three separate experiments (at least 30 images for each condition and experiment were analysed). Significance between PLAN1 and control iNs is represented as ***p-value <0.001. Significance between vitamin E (50 μM) treated and untreated lines is represented as [a]p-value <0.001. (For interpretation of the references to colour in this figure legend, the reader is referred to the web version of this article.)

mediated lipid peroxidation (Jiang et al., 2021; Kajarabille and Latunde-Dada, 2019; Li et al., 2020; Xie et al., 2016). The enhancement of cell viability in PLAN fibroblasts by vitamin E, in presence of Luperox®, may indicate that cell death is caused by ferroptosis. This hypothesis needs to be confirmed by further research.

In summary, the present work supports the hypothesis that patients-derived PLAN fibroblasts are a promising model for the study of disease pathophysiology and the evaluation of potential therapies. Fibroblasts and iNs harbouring *PLA2G6* mutations manifest excess lipid peroxidation and ROS production, iron/lipofuscin accumulation and impaired ΔΨm. Our results also indicate that iNs can reproduce the main pathological alterations of the disease and are also a useful tool for disease modelling. The role of lipid peroxidation in iron and lipofuscin accumulation suggests that this process is a main therapeutic target. To this

respect, we show the protective effect of vitamin E supplementation on the main pathological alterations in both cellular models. These findings suggest that blockage of lipid peroxidation by vitamin E treatment alleviates PLAN cellular alterations. However, further studies are needed to completely elucidate the pathophysiological mechanisms of the disease and to assess the potential utility of Vitamin E or other membrane antioxidants in PLAN therapy.

Author's roles

Conceptualization, J.A. Sánchez-Alcázar and I. Villalón-García; execution, I. Villalón-García, M. Alvarez-Cordoba, M. Talaverón-Rey, S. Povea-Cabello, J.J. Salas, J. M, Suárez-Rivero, M. Villanueva-Paz and Raquel Luzón-Hidalgo; electrophysiological recordings, A. Rodríguez-Moreno and R. Falcón-Moya; electron microscopy, J.A. Armengol; formal analysis, I. Villalón-García, A. Suárez-Carrillo, and M. Munuera-Cabeza; writing-original draft preparation, I, Villalón-Garcia; writing-review and editing, J. A. Sánchez-Alcázar; funding acquisition, J.A. Sánchez-Alcázar. All authors have read and agreed to the published version of the manuscript.

Funding disclosure

This work was supported by FIS PI16/00786 and PI19/00377 grants, Instituto de Salud Carlos III, Spain and Fondo Europeo de Desarrollo Regional (FEDR-Unión Europea), Proyectos de Investigación de Excelencia de la Junta de Andalucía CTS-5725 and PY18-850 and by AIDNAI (Association Internationale de Dystrophie Neuro Axonale Infantile), ENACH (Asociación de Enfermos de Neurodegeneración con Acumulación Cerebral de Hierro), AEPMI (Asociación de Enfermos de Patología Mitocondrial), FEDER (Federación Española de Enfermedades Raras) and Fundación MERK Salud. S. Povea-Cabello is a recipient of Ayudas para la Formación del Profesorado Universitario (FPU) from Ministerio de Universidades de España.

Competing interests

The authors declare that they have no competing interests.

Consent to participate

The study was approved by The Ethical Committee of Hospital Universitario Virgen del Rocío and Virgen Macarena of Seville, protocol code BRAINCURE16, following the Spanish laws, the principles of the Declaration of Helsinki, and the Guideline for Good Clinical Practices.

CRediT authorship contribution statement

Irene Villalón-García: Conceptualization, Methodology, Formal analysis, Investigation. **Mónica Álvarez-Córdoba:** Investigation. **Suleva Povea-Cabello:** Investigation, Methodology. **Marta Talaverón-Rey:** Investigation. **Marina Villanueva-Paz:** Investigation, Methodology. **Raquel Luzón-Hidalgo:** Investigation. **Juan M. Suárez-Rivero:** Investigation, Formal analysis. **Alejandra Suárez-Carrillo:** Investigation, Methodology. **Manuel Munuera-Cabeza:** Investigation. **Joaquín J. Salas:** Investigation. **Rafael Falcón-Moya:** Investigation. **Antonio Rodríguez-Moreno:** Investigation, Methodology. **José A. Armengol:** Investigation. **José A. Sánchez-Alcázar:** Conceptualization, Writing – review & editing, Funding acquisition.

Acknowledgments

We thank María Pilar Burgos Domenech from Instituto de Recursos Naturales y Agrobiología de Sevilla for her contributions with the ICP-MS assays. We also thank Dr. Malin Parmar group, from Lund University for providing the plasmids and knowledge on direct reprogramming technology. Funding for open access publishing: Universidad Pablo de Olavide/CBUA.

Appendix A. Supplementary data

Supplementary data to this article can be found online at https://doi.org/10.1016/j.nbd.2022.105649.

References

Adams, D., et al., 2020. Treatment of infantile neuroaxonal dystrophy with RT001: a di-deuterated ethyl ester of linoleic acid: report of two cases. JIMD Rep. 54, 54–60.
Akiba, S., Sato, T., 2004. Cellular function of calcium-independent phospholipase A2. Biol. Pharm. Bull. 27, 1174–1178.
Alcocer-Gómez, E., et al., 2015. Metformin and caloric restriction induce an AMPK-dependent restoration of mitochondrial dysfunction in fibroblasts from fibromyalgia patients. Biochim. Biophys. Acta 1852, 1257–1267.
Álvarez-Córdoba, M., et al., 2018. Pantothenate rescues iron accumulation in pantothenate kinase-associated neurodegeneration depending on the type of mutation. Mol. Neurobiol. 56, 3638–3656.
Aoun, M., Tiranti, V., 2015. Mitochondria: a crossroads for lipid metabolism defect in neurodegeneration with brain iron accumulation diseases. Int. J. Biochem. Cell Biol. 63.
Arber, C., et al., 2016. Insights into molecular mechanisms of disease in neurodegeneration with brain iron accumulation: unifying theories. Neuropathol. Appl. Neurobiol. 42, 220–241.
Aring, L., et al., 2020. WDR45 contributes to Iron accumulation through dysregulation of neuronal Iron homeostasis. Curr. Dev. Nutr. 4.
Balboa, M.A., et al., 2002. Expression and function of phospholipase A2 in brain. FEBS Lett. 531, 12–17.
Balsinde, J., Balboa, M.A., 2005. Cellular regulation and proposed biological functions of group VIA calcium-independent phospholipase A2 in activated cells. Cell. Signal. 17, 1052–1062.
Beck, G., et al., 2011. Neuroaxonal dystrophy in calcium-independent phospholipase A2 deficiency results from insufficient remodeling and degeneration of mitochondrial and presynaptic membranes. J. Neurosci. 31, 11411–11420.
Beck, G., et al., 2016. Deficiency of calcium-independent phospholipase A2 Beta induces brain Iron accumulation through upregulation of divalent metal transporter 1. PLoS One 10.
Brunk, U.T., Terman, A., 2002. The mitochondrial-lysosomal axis theory of aging. Accumulation of damaged mitochondria as a result of imperfect autophagocytosis. Eur. J. Biochem. 269, 1996–2002.
Butterfield, D.A., et al., 2002. Vitamin E and neurodegenerative disorders associated with oxidative stress. Nutr. Neurosci. 5, 229–239.
Campanella, A., et al., 2012. Skin fibroblasts from pantothenate kinase-associated neurodegeneration patients show altered cellular oxidative status and have defective iron-handling properties. Hum. Mol. Genet. 21, 4049–4059.
Ching-Chi, C., et al., 2017. PARK14 PLA2G6 mutants are defective in preventing rotenoneinduced mitochondrial dysfunction, ROS generation and activation of mitochondrial apoptotic pathway. Oncotarget 8, 79046–79060.
Cho, S., Hwang, E.S., 2011. Chapter 7 - fluorescence-based detection and quantification of features of cellular senescence. In: Darzynkiewicz, Z., et al. (Eds.), Methods in Cell Biology. Academic Press, pp. 149–188.
Cho, K.A., et al., 2004. Morphological adjustment of senescent cells by modulating Caveolin-1 status. J. Biol. Chem. 279, 42270–42278.
Chow, C.K., 2001. Vitamin E regulation of mitochondrial superoxide generation. Biol. Signals Recept. 19, 112–124.
Cif, L., et al., 2014. Atypical PLA2G6-associated neurodegeneration: social communication impairment, dystonia and response to deep brain stimulation. Mov. Disord. Clin Pract. 1, 128–131.
Dang, T.N., et al., 2010. The putative heme transporter HCP1 is expressed in cultured astrocytes and contributes to the uptake of hemin. Glia. 58, 55–65.
Davids, M., et al., 2016. Disruption of Golgi morphology and altered protein glycosylation in PLA2G6-associated neurodegeneration. J. Med. Genet. 53, 180–189.
de Figueiredo, P., et al., 2000. Phospholipase A2 antagonists inhibit constitutive retrograde membrane traffic to the endoplasmic reticulum. Traffic 1, 504–511.
Defendini, R., et al., 1973. Hallervorden-Spatz disease and infantile neuroaxonal dystrophy. Ultrastructural observations, anatomical pathology and nosology. J. Neurol. Sci. 20, 7–23.
Drouin-Ouellet, J., et al., 2017. REST suppression mediates neural conversion of adult human fibroblasts via microRNA-dependent and -independent pathways. EMBO Mol. Med. 9, 1117–1131.
Escárcega, R.D., 2019. El aumento de Ca2+ intracelular modifica la distribución de las proteínas de fusión, y la morfología mitocondrial en las neuronas y astrocitos. Centro de Investigaciones Cerebrales. Universidad Veracruzana. Centro de Investigaciones Cerebrales, Veracruz.
Evangelou, K., Gorgoulis, V.G., 2017. Sudan Black B, the specifi c histochemical stain for lipofuscin: a novel method to detect senescent cells. Methods Mol. Biol. 1534, 111–119.
Ferese, R., et al., 2018. Heterozygous PLA2G6 mutation leads to Iron accumulation within basal ganglia and Parkinson's disease. Front. Neurol. 9, 536.
Frolova, M., et al., 2015. Degradation of mitochondria to lipofuscin upon heating and illumination. Biophysics 60, 1125–1131.

Georgakopoulou, E., et al., 2013. Specific lipofuscin staining as a novel biomarker to detect replicative and stress-induced senescence. A method applicable in cryo-preserved and archival tissues. Aging. 5, 37–50.
González-Gualda, E., et al., 2021. A guide to assessing cellular senescence in vitro and in vivo. FEBS J. 288, 56–80.
Gregory, A., Hayflick, S.J., 2005. Neurodegeneration with brain iron accumulation. Folia Neuropathol. 43, 286–296.
Gregory, A., Hayflick, S., 2013. Neurodegeneration with brain iron accumulation disorders overview. In: Adam, M., et al. (Eds.), GeneReviews® [Internet]. University of Washington, Seattle, Seattle (WA).
Gregory, A., et al., 2008. PLA2G6-associated neurodegeneration. In: Adam, M., et al. (Eds.), GeneReviews® [Internet]. University of Washington, Seattle, Seattle (WA).
Gregory, A., et al., 2009. Clinical and genetic delineation of neurodegeneration with brain iron accumulation. J. Med. Genet. 46, 73–80.
Guo, Y.P., et al., 2019. Impaired iPLA2β activity affects iron uptake and storage without iron accumulation: an in vitro study excluding decreased iPLA2β activity as the cause of iron deposition in PLAN. Brain Res. 1712, 25–33.
Hayflick, L., Moorhead, P., 1961. The serial cultivation of human diploid cell strains. Exp. Cell Res. 25, 585–621.
Hayflick, S.J., et al., 2018. Neurodegeneration with brain iron accumulation. Handb. Clin. Neurol. 147, 293–305.
Hinarejos, I., et al., 2020. Mitochondrial dysfunction, oxidative stress and neuroinflammation in neurodegeneration with brain iron accumulation (NBIA). Antioxidants 9.
Höhn, A., Grune, T., 2013. Lipofuscin: formation, effects and role of macroautophagy. Redox Biol. 1, 140–144.
Iankova, V., et al., 2021. Emerging disease-modifying therapies in neurodegeneration with brain Iron accumulation (NBIA) disorders. Front. Neurol. 12.
Iliadi, K.G., et al., 2018. Mutations in the Drosophila homolog of human PLA2G6 give rise to age-dependent loss of psychomotor activity and neurodegeneration. Sci. Rep. 8.
Illingworth, M., et al., 2014. PLA2G6-associated neurodegeneration (PLAN): further expansion of the clinical, radiological and mutation spectrum associated with infantile and atypical childhood-onset disease. Mol. Genet. Metab. 112, 183–189.
Ingrassia, R., et al., 2017. Ferrous iron up-regulation in fibroblasts of patients with beta propeller protein-associated neurodegeneration (BPAN). Front. Genet. 8, 18.
Jiang, X., et al., 2021. Ferroptosis: mechanisms, biology and role in disease. Nat. Rev. Mol. Cell Biol. 22, 266–282.
Johri, A., Beal, M.F., 2012. Antioxidants in Huntington's disease. Biochim. Biophys. Acta 1822, 664–674.
Kajarabille, N., Latunde-Dada, G.O., 2019. Programmed cell-death by ferroptosis: antioxidants as mitigators. Int. J. Mol. Sci. 20.
Karin, I., et al., 2021. Treat Iron-related childhood-onset neurodegeneration (TIRCON)—an international network on care and research for patients with neurodegeneration with brain Iron accumulation (NBIA). Front. Neurol. 12.
Kinghorn, K.J., et al., 2015. Loss of PLA2G6 leads to elevated mitochondrial lipid peroxidation and mitochondrial dysfunction. Brain 138, 1801–1816.
Kinghorna, K.J., Castillo-Quana, J.I., 2016. Mitochondrial dysfunction and defects in lipid homeostasis as therapeutic targets in neurodegeneration with brain iron accumulation. Rare Dis. 4, e1128616.
Krohne, T.U., et al., 2010. Effects of lipid peroxidation products on lipofuscinogenesis and autophagy in human retinal pigment epithelial cells. Exp. Eye Res. 90, 465–471.
Kurz, T., et al., 2008. Lysosomes in iron metabolism, ageing and apoptosis. Histochem. Cell Biol. 129, 389–406.
Levi, S., Finazzi, D., 2014. Neurodegeneration with brain iron accumulation: update on pathogenic mechanisms. Front. Pharmacol. 5.
Levi, S., Tiranti, V., 2019. Neurodegeneration with brain Iron accumulation disorders: valuable models aimed at understanding the pathogenesis of Iron deposition. Pharmaceuticals 12, 27.
Li, J., et al., 2020. Ferroptosis: past, present and future. Cell Death Dis. 11, 88.
Merrill, R.A., et al., 2017. Measuring mitochondrial shape with ImageJ. In: Strack, S., Usachev, Y. (Eds.), Techniques to Investigate Mitochondrial Function in Neurons. Humana Press, New York, NY, pp. 31–48.
Milner, P., 2018. Clinical Trials. A Study to Assess Efficacy and Safety of RT001 in Subjects With Infantile Neuroaxonal Dystrophy.
Milward, E., et al., 2012. Brain changes in iron loading disorders. In: Linert, W., Kozlowski, H. (Eds.), Metal Ions in Neurological Systems. Springer-Verlag, Vienna, pp. 17–29.
Moreno-García, A., et al., 2018. An overview of the role of lipofuscin in age-related neurodegeneration. Front. Neurosci. 12.
Morgan, N.V., et al., 2006. PLA2G6, encoding a phospholipase A2, is mutated in neurodegenerative disorders with high brain iron. Nat. Genet. 38, 752–754.
Mustacich, D.J., et al., 2007. Vitamin E. Vitam. Horm. 76, 1–21.
Neurohr, G.E., et al., 2019. Excessive cell growth causes cytoplasm dilution and contributes to senescence. Cell 176, 1083–1097.
Niki, E., 2014. Role of vitamin E as a lipid-soluble peroxyl radical scavenger: in vitroand in vivo evidence. Free Radic. Biol. Med. 66, 3–12.
Pap, E., et al., 1999. Ratio-fluorescence microscopy of lipid oxidation in living cells using C11-BODIPY(581/591). FEBS Lett. 453, 278–282.
Park, B.E., et al., 1975. Pathogenesis of pigment and spheroid formation in Hallervorden-Spatz syndrome and related disorders. Neurology 25, 1172–1178.
Powell, S.R., et al., 2005. Aggregates of oxidized proteins (lipofuscin) induce apoptosis through proteasome inhibition and dysregulation of proapoptotic proteins. Free Radic. Biol. Med. 38, 1093–1101.
Riemer, J., et al., 2004. Colorimetric ferrozine-based assay for the quantitation of iron in cultured cells. Anal. Biochem. 331, 370–375.
Rockfield, S., et al., 2018. Links between Iron and lipids: implications in some major human diseases. Pharmaceuticals 11.
Rodríguez-Hernández, Á., et al., 2009. Coenzyme Q deficiency triggers mitochondria degradation by mitophagy. Autophagy 5, 19–32.
Santambrogio, P., et al., 2015. Mitochondrial iron and energetic dysfunction distinguish fibroblasts and induced neurons from pantothenate kinase-associated neurodegeneration patients. Neurobiol. Dis. 81, 144–153.
Seleznev, K., et al., 2006. Calcium-independent phospholipase A2 localizes in and protects mitochondria during apoptotic induction by staurosporine. J. Biol. Chem. 281, 22275–22288.
Shioji, K., et al., 2010. Synthesis and properties of fluorescence probe for detection of peroxides in mitochondria. Bioorg. Med. Chem. Lett. 20, 3911–3915.
Shrigley, S., et al., 2018. Simple generation of a high yield culture of induced neurons from human adult skin fibroblasts. J. Vis. Exp. 132.
Sitte, N., et al., 2000. Proteasome inhibition by lipofuscin/ceroid during postmitotic aging of fibroblasts. FASEB J. 14, 1490–1498.
Strober, W., 2015. Trypan blue exclusion test of cell viability. Curr. Protoc. Immunol. 111. A3.B.1–A3.B.3.
Sumi-Akamaru, H., et al., 2015. Neuroaxonal dystrophy in PLA2G6 knockout mice. Neuropathology. 35, 289–302.
Surowka, A.D., et al., 2014. A methodological approach to the characterization of brain gliomas by means of semi-authomatic morhometric analysis. Image Anal. Stereol. 33, 1–18.
Tarohda, T., et al., 2005. Regional distributions of manganese, iron, copper, and zinc in the brains of 6-hydroxydopamine-induced parkinsonian rats. Anal. Bioanal. Chem. 383, 224–234.
Tomiyama, H., et al., 2011. PLA2G6 variant in Parkinson's disease. J. Hum. Genet. 56, 401–403.
Ulatowski, L.M., Manor, D., 2015. Vitamin E and neurodegeneration. Neurobiol. Dis. 84, 78–83.
Villanueva-Paz, M., et al., 2019. Pathophysiological characterization of MERRF patient-specific induced neurons generated by direct reprogramming. Biochim. Biophys. Acta, Mol. Cell Res. 1866, 861–881.
Villanueva-Paz, M., et al., 2020. Parkin-mediated mitophagy and autophagy flux disruption in cellular models of MERRF syndrome. Biochim. Biophys. Acta Mol. basis Dis. 1866.
Xie, Y., et al., 2016. Ferroptosis: process and function. Cell Death Differ. 23, 369–379.
Yin, H., et al., 2011. Free radical lipid peroxidation: mechanisms and analysis. Chem. Rev. 11, 5944–5972.
Yoshino, H., et al., 2010. Phenotypic spectrum of patients with PLA2G6 mutation and PARK14-linked parkinsonism. Neurology 75, 1356–1361.
Yu, T., et al., 2006. Increased production of reactive oxygen species in hyperglycemic conditions requires dynamic change of mitochondrial morphology. Proc. Natl. Acad. Sci. U. S. A. 103, 2653–2658.
Zhao, T., et al., 2021. Iron accumulation and lipid peroxidation in the aging retina: implication of ferroptosis in age-related macular degeneration. Aging Dis. 12, 529–551.
Zhou, Q., et al., 2014. Impairment of PARK14-dependent Ca2þ signalling is a novel determinant of Parkinson's disease. Nat. Commun. 7.
Zufferey, R., et al., 1997. Multiply attenuated lentiviral vector achieves efficient gene delivery in vivo. Nat. Biotechnol. 15, 871–875.